Cell

Cancer Vulnerabilities Unveiled by Genomic Loss

Deepak Nijhawan,[1,2,7,9,10] Travis I. Zack,[1,2,3,9] Yin Ren,[5] Matthew R. Strickland,[1] Rebecca Lamothe,[1] Steven E. Schumacher,[1,2] Aviad Tsherniak,[2] Henrike C. Besche,[4] Joseph Rosenbluh,[1,2,7] Shyemaa Shehata,[1] Glenn S. Cowley,[2] Barbara A. Weir,[2] Alfred L. Goldberg,[4] Jill P. Mesirov,[2] David E. Root,[2] Sangeeta N. Bhatia,[2,5,6,7,8] Rameen Beroukhim,[1,2,7,*] and William C. Hahn[1,2,7,*]

[1]Departments of Cancer Biology and Medical Oncology, Dana Farber Cancer Institute, Boston, MA 02215, USA
[2]Broad Institute of Harvard and MIT, Cambridge, MA 02142, USA
[3]Biophysics Program, Harvard University, Boston, MA 02115, USA
[4]Department of Cell Biology, Harvard Medical School, 240 Longwood Avenue, Boston, MA 02115, USA
[5]Harvard-MIT Division of Health Sciences and Technology
[6]David H. Koch Institute for Integrative Cancer Research
Massachusetts Institute of Technology, Cambridge, MA 02139, USA
[7]Department of Medicine, Brigham and Women's Hospital and Harvard Medical School, Boston, MA 02115, USA
[8]Howard Hughes Medical Institute, Chevy Chase, MD 20815, USA
[9]These authors contributed equally to this work
[10]Present address: Division of Hematology and Oncology, Department of Internal Medicine, University of Texas Southwestern Medical Center, Dallas, TX 75390, USA
*Correspondence: rameen_beroukhim@dfci.harvard.edu (R.B.), william_hahn@dfci.harvard.edu (W.C.H.)
http://dx.doi.org/10.1016/j.cell.2012.07.023

SUMMARY

Due to genome instability, most cancers exhibit loss of regions containing tumor suppressor genes and collateral loss of other genes. To identify cancer-specific vulnerabilities that are the result of copy number losses, we performed integrated analyses of genome-wide copy number and RNAi profiles and identified 56 genes for which gene suppression specifically inhibited the proliferation of cells harboring partial copy number loss of that gene. These CYCLOPS (*c*opy number alterations *y*ielding *c*ancer *l*iabilities *o*wing to *p*artial loss) genes are enriched for spliceosome, proteasome, and ribosome components. One CYCLOPS gene, *PSMC2*, encodes an essential member of the 19S proteasome. Normal cells express excess PSMC2, which resides in a complex with PSMC1, PSMD2, and PSMD5 and acts as a reservoir protecting cells from *PSMC2* suppression. Cells harboring partial *PSMC2* copy number loss lack this complex and die after *PSMC2* suppression. These observations define a distinct class of cancer-specific liabilities resulting from genome instability.

INTRODUCTION

Cancers arise as the result of the accumulation of somatic genetic alterations within a cell, including chromosome translocations, single base substitutions, and copy number alterations (Stratton et al., 2009). Although a subset of these alterations ("driver events") promote malignant transformation by activating oncogenes or inactivating tumor suppressor genes, most somatic genetic alterations are the consequence of increased genomic instability that occurs in cancer but does not contribute to tumor development ("passenger events").

The demonstration that cancers are often dependent on specific driver oncogenes has stimulated efforts to find and exploit these targets therapeutically. For example, cancers that harbor translocations that form fusion transcripts such as BCR-ABL or EML4-ALK or mutations such as EGFR or BRAF depend on the activity of these gene products for tumor maintenance (Brose et al., 2002; Daley et al., 1990; Soda et al., 2007). Therefore, the presence of such an alteration often predicts response to drugs that inhibit the function of these proteins (Sawyers, 2005).

An alternative strategy to target cancers is to target genes that are not oncogenes but are genes that cancers require to accommodate cancer-specific stress (Ashworth et al., 2011; Kaelin, 2005). In comparison to normal cells, cancer cells rely inordinately on pathways that abrogate a variety of cancer-related stressors that include DNA damage replication stress, proteotoxic stress, mitotic stress, metabolic stress, and oxidative stress (Solimini et al., 2007). Even though proteins within these pathways may be essential in all cells, genetic alterations may induce a state in which reliance on these pathways creates a therapeutic window as a result of cancer-specific stresses.

The proteasome, which recognizes and degrades proteins modified with a polyubiquitin chain (Finley, 2009), is one such target. Although proteasome function is essential to cells for basal protein turnover and for degradation of unfolded proteins, multiple myeloma cells produce excessive amounts of immunoglobulin and appear to be especially dependent on effective protein turnover by the 26S proteasome. Indeed, the 20S

proteasome inhibitor bortezomib is used as first-line treatment of multiple myeloma (Richardson et al., 2005).

Genomic instability may be another source of cancer-specific stress. The majority of human cancers harbor copy number alterations involving the loss or gain of broad chromosomal regions. For example, copy number losses that target tumor suppressor genes often involve multiple neighboring genes that may not contribute to cancer development. The loss of such neighboring genes has been postulated to render cancer cells highly vulnerable to further suppression or inhibition of those genes (Frei, 1993), but until recently, the tools to systematically test this hypothesis were not available. Here, we integrated both genome-scale copy number and loss-of-function data on a panel of 86 cancer cell lines to determine whether partial copy number loss of specific genes renders cells highly dependent on the remaining copy. We identified a class of genes enriched for cell-essential genes, most predominantly proteasome, spliceosome, and ribosome components, which render cells that harbor copy number loss highly dependent on the expression of the remaining copy.

RESULTS

Integration of Genome-Scale Copy Number and Gene Dependency Analyses Identifies CYCLOPS Genes

By analyzing copy number profiles from 3,131 cancers across a wide diversity of cancer types (Beroukhim et al., 2010), we found that most cancers exhibit copy number loss affecting at least 11% of the genome and that many cancers exhibit much more extensive loss of genetic material (Figure 1A). Much of this widespread genomic disruption is due to copy number alterations involving whole chromosomes or chromosome arms, presumably due to mechanisms that favor the generation of such large events (Figure 1B). As a consequence, most genes undergo copy number loss in a substantial fraction of cancers (average, 16.2; range, 3.7%–40.2%; Figure S1A available online). A subset of the genes affected by recurrent copy number losses contributes to cancer development as tumor suppressor genes; however, many genes are recurrently lost due to passenger events or because of their proximity to a frequently deleted tumor suppressor gene (Figures 1C and S1B). We hypothesized that, for a subset of nondriver genes, hemizygous loss may be tolerated and frequent, but complete loss would lead to cell death. In some of these cases, hemizygous loss might lead to sensitivity to further suppression of the gene relative to cells without copy number loss of these genes.

To identify genes whose loss correlated with a greater sensitivity to further gene suppression, we integrated gene dependencies and copy number data from 86 cancer cell lines (Table S1). We analyzed gene essentiality data from Project Achilles, a data set that scored the impact of individually expressing 54,020 short hairpin RNAs (shRNAs) targeting 11,194 genes on the proliferation of 102 cell lines (Cheung et al., 2011). For 7,250 of these genes, multiple shRNAs had comparable effects across cell lines, suggesting that their effects were due to suppression of the intended target. We used these shRNAs to construct composite "gene dependency scores" (A.T., W.C.H., and J.P.M., unpublished data). We also obtained DNA copy numbers for these same cell lines from Affymetrix SNP 6.0 array data (Barretina et al., 2012). For each gene, we first classified each cell line by whether or not it exhibited copy number loss in that gene and then calculated the mean gene dependency score among cell lines in each class. We then determined the difference in mean scores between the copy-loss and copy-neutral classes and rated the significance of this difference by permuting class labels (Figure 1D). To minimize the confounding effect of lineage, all permutations maintained the initial lineage distribution within each class. We also restricted these analyses to the 5,312 genes for which each class contained at least seven cell lines. We identified 56 candidate genes with false discovery rate (FDR) (Benjamini and Hochberg, 1995) p values of less than 0.25 (Tables 1 and S2) and named them CYCLOPS (*c*opy number alterations *y*ielding *c*ancer *l*iabilities *o*wing to *p*artial loss) genes.

We validated the CYCLOPS vulnerabilities by using an independently generated RNA interference (RNAi) data set (shRNA Activity Rank Profile, shARP) (Marcotte et al., 2012) representing the consequences of expressing 78,432 shRNAs targeting 16,056 genes on the proliferation of 72 breast, ovarian, or pancreatic cancer cell lines. We applied the same analysis pipeline, which was constrained to the "validation set" of 47 cell lines for which we had copy number data and the 6,574 genes for which at least seven cell lines were in each class (copy loss and copy neutral) (Tables S1 and S2). These genes included 3,282 of the genes that underwent full analysis in the Achilles data set and 40 of the CYCLOPS candidates identified in that analysis. Although the lineage distribution was markedly different between the validation and Achilles data sets (breast and pancreatic cancers made up 90% of the cell lines in the validation set but only 15% in Project Achilles), the 40 CYCLOPS candidates identified in the Achilles analysis were also among the most significant genes in the shARP analysis (Kolomogorov-Smirnov [KS] statistic, $p = 2 \times 10^{-9}$).

Features of CYCLOPS Genes

In copy number analyses collected from 3,131 tumor samples and cancer cell lines (Beroukhim et al., 2010), each CYCLOPS candidate exhibited hemizygous loss in an average of 18.5% of samples (range, 8%–33%), which was as common as for the other 5,256 genes in the analysis (average, 17.7%; range, 4%–34%; two-tailed permutation test, $p = 0.17$). In contrast, CYCLOPS genes exhibited much lower rates of homozygous deletion ($p = 0.02$) and DNA methylation ($p = 0.026$) (Figure 1E). This observation suggested that CYCLOPS genes are enriched for genes required for cell proliferation or survival.

We also found that CYCLOPS candidates are highly enriched among 1,336 human genes that are homologous to the set of genes found to be essential in *S. cerevisiae* (Zhang and Lin, 2009) ($p < 0.0001$) and that exhibit comparable rates of genetic and epigenetic alterations (Table S3). A pathway enrichment analysis showed that the spliceosome, proteasome, and ribosome were the most highly enriched pathways among CYCLOPS candidates (KS statistic FDR = 1.4×10^{-8}, 2.7×10^{-5}, and 1.8×10^{-4}, respectively) and in our analysis of the validation set (FDR = 3.1×10^{-15}, 1.5×10^{-12}, and 2.3×10^{-17}, respectively). Together, these observations indicate that CYCLOPS genes are a unique subset of cell-essential genes

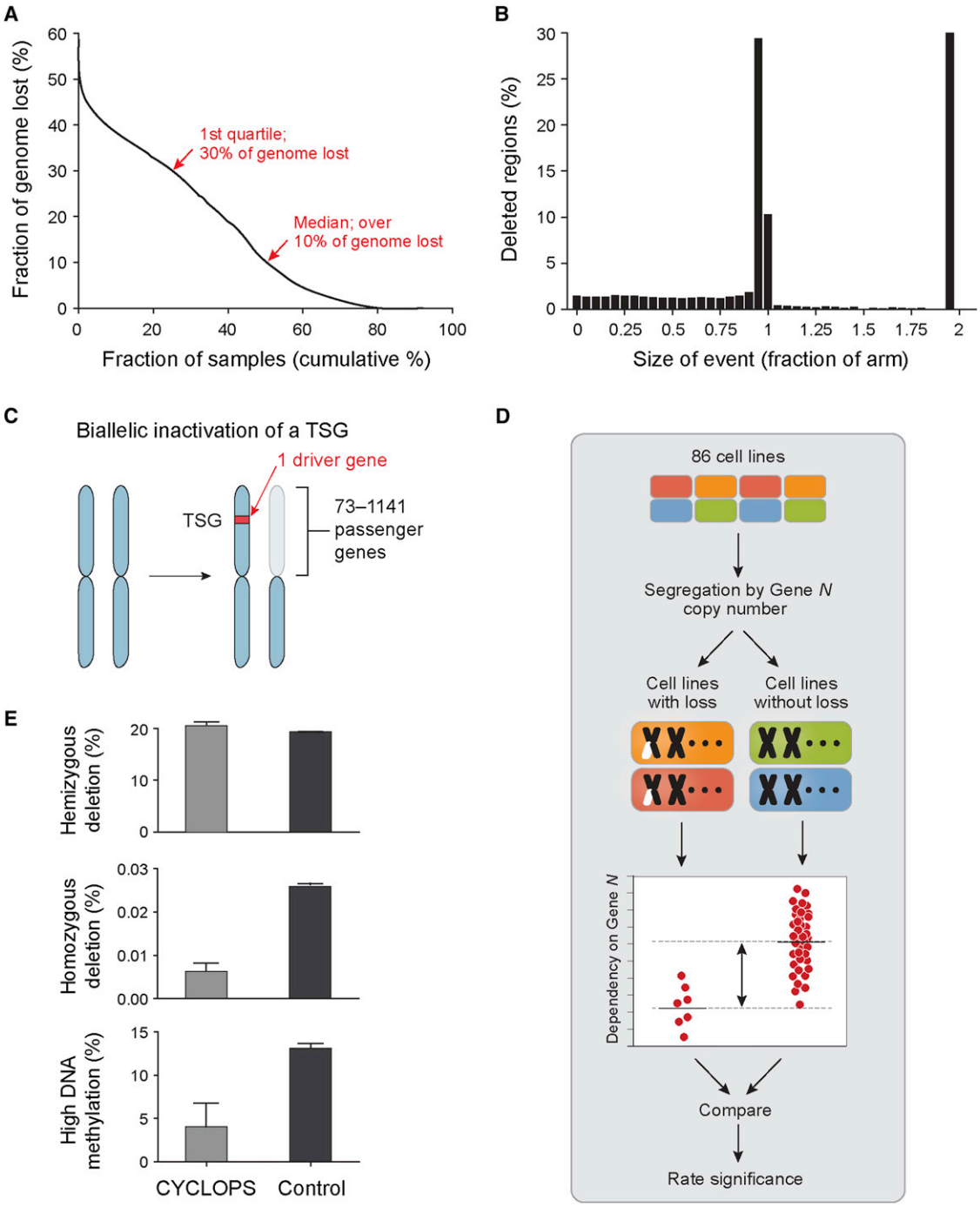

Figure 1. Identification of CYCLOPS Genes

(A) The percentage of the cancer genome involved in copy number loss.

(B) The fraction of deleted regions associated with deletion events of varying lengths.

(C) Biallelic inactivation of a tumor suppressor is often associated with a focal alteration of one copy (red bar) and hemizygous loss of all genes on the chromosome arm containing the other copy.

(D) Schematic describing the approach to identifying CYCLOPS genes. For each gene, we separated cell lines with and without loss of the gene and compared their dependency on that gene by permuting class labels.

(E) Frequency of hemizygous deletion, homozygous deletion, or DNA methylation of CYCLOPS and other genes.

Data are presented as averages ±SEM. See also Figure S1 and Tables S1, S2, and S3.

Table 1. Top-Ranked CYCLOPS Candidates and Frequency of Partial Genomic Loss in 3,131 Tumors

Gene	Band	FDR Value	Frequency of Loss
PSMC2[a]	7q22.1	0.03	0.10
EIF2B2	14q24.3	0.03	0.17
EEF2	19p13.3	0.03	0.27
PHF5A[b]	22q13.2	0.03	0.23
HPGD	4q34.1	0.03	0.26
RPS15[c]	19p13.3	0.03	0.28
SNRPB[b]	20p13	0.03	0.13
POLR2F	22q13.1	0.03	0.22
USPL1	13q12.3	0.05	0.27
SMC2	9q31.1	0.07	0.21
SMU1	9p13.3	0.08	0.25
PUF60[b]	8q24.3	0.08	0.08
RPS11[c]	19q13.33	0.08	0.19
POLG	15q26.1	0.08	0.17
ZNF583	19q13.43	0.08	0.20
CPT1B	22q13.31	0.08	0.25
BMP8A	1p34.2	0.09	0.12
TIE1	1p34.2	0.09	0.11
SF3A2[b]	19p13.3	0.09	0.27
SNRNP70[b]	19q13.33	0.09	0.19
RBM17[b]	10p15.1	0.09	0.20
PCNA	20p12.3	0.09	0.12
PSMA4[a]	15q25.1	0.09	0.18
LSM4[b]	19p13.11	0.09	0.20
EEF1A1	6q13	0.12	0.20

[a]Proteasome KEGG Pathway designation.
[b]Spliceosome KEGG Pathway designation.
[c]Ribosome KEGG Pathway designation.

for which partial, but not complete, suppression is compatible with cancer cell viability.

These observations led us to hypothesize that copy number loss might unveil vulnerabilities in CYCLOPS genes through decreased gene expression. We therefore evaluated the relation between copy number loss and expression by using integrated SNP and expression data for 16,767 and 11,118 genes, respectively, in two panels of samples: the Cancer Cell Line Encyclopedia (CCLE of 806 cell lines across 24 cancer types) (Barretina et al., 2012) and 429 ovarian cancers profiled by The Cancer Genome Atlas (TCGA) Project (Cancer Genome Atlas Research Network, 2011). We found that the average strength of correlation between copy number loss and messenger RNA (mRNA) expression was significantly higher for CYCLOPS candidates than for the other genes in our analysis (CCLE, $r = 0.39$ versus 0.26, $p < 0.0001$; TCGA, $r = 0.44$ versus 0.34, $p = 0.0017$; Figure S1C).

PSMC2 Is a CYCLOPS Gene

PSMC2 (*Rpt1*) was the highest-ranked CYCLOPS candidate in our original analysis and was also significant in the validation data set. PSMC2 is part of the 19S regulatory complex of the 26S proteasome, which is responsible for catalyzing the unfolding and translocation of substrates into the 20S proteasome (Smith et al., 2011). Either one or two 19S regulatory complexes combine with a single 20S catalytic complex to form, respectively, a singly or doubly capped ($26S^1$ or $26S^2$) complete 26S proteasome (Finley, 2009). PSMC2 expression is essential for 19S and 26S proteasome assembly (Kaneko et al., 2009).

To minimize the possibility that other genetic alteration(s) confounded our analyses, we determined whether expression or copy number levels of every other gene for which we had data showed significant correlations with *PSMC2* sensitivity. Low *PSMC2* expression (FDR < 0.017) and *PSMC2* copy number loss (FDR < 0.008) were the features most significantly correlated with *PSMC2* sensitivity (Table S4). Conversely, among the 7,250 genes in our Achilles analysis, sensitivity to *PSMC2* was the only feature that correlated with *PSMC2* copy number loss (FDR < 0.25; Table S5). In particular, among all 47 other proteasome components surveyed, neither expression levels nor copy number status significantly correlated with *PSMC2* sensitivity. We also found no evidence that suppression of any of the other proteasome components inhibited the proliferation of cell lines with *PSMC2* copy number loss. The association between *PSMC2* copy number loss and *PSMC2* sensitivity also remained significant when cells with *PSMC2* copy number gains were excluded from the analysis ($p = 0.0006$).

To estimate the differential sensitivity of cell lines harboring normal copies or copy number loss of *PSMC2* to gene suppression, we compared the effects of *PSMC2* suppression to that observed when we suppressed the oncogenes *KRAS*, *PIK3CA*, and *BRAF*. In consonance with prior studies (Weinstein and Joe, 2006), suppression of these oncogenes inhibited proliferation of cells harboring mutated and constitutively active oncogenes compared to cells expressing wild-type proto-oncogenes ($p < 2 \times 10^{-5}$ in each case) (Figure 2A). However, the difference in *PSMC2* dependency scores between cell lines with and without *PSMC2* copy number loss ($PSMC2^{Loss}$ and $PSMC2^{Neutral}$, respectively) was greater than for any of these oncogenes (Figure 2A).

We confirmed the vulnerability of $PSMC2^{Loss}$ lines to *PSMC2* suppression in a direct competition assay by comparing the proliferation rate of uninfected cells to cells that coexpress green fluorescent protein (GFP) and either shLacZ or a *PSMC2*-specific shRNA (Figure S2A) in six ovarian cell lines over 21 days. The expression of shLacZ or *PSMC2* shRNAs did not induce significant changes in the proliferation of $PSMC2^{Neutral}$ cells, including two ovarian cancers and one nontransformed immortalized ovarian surface epithelial (IOSE) cell line (Liu et al., 2004) (Figure 2B). After 21 days of culture, PSMC2 levels remained suppressed in $PSMC2^{Neutral}$ cells that constitutively express *PSMC2* shRNA, which is consistent with the lack of an observed proliferation deficit (Figure S2B). In contrast, expression of *PSMC2* shRNAs in $PSMC2^{Loss}$ cells was not compatible with long-term culture and reduced the proliferation rate by at least 50% in all three $PSMC2^{Loss}$ ovarian cancer cell lines within 7 days (Figure 2B).

To confirm that these observations were due to the suppression of *PSMC2*, we expressed an N-terminal V5-epitope-tagged form of *PSMC2* (hereafter referred to as *V5-PSMC2*) in OVCAR8,

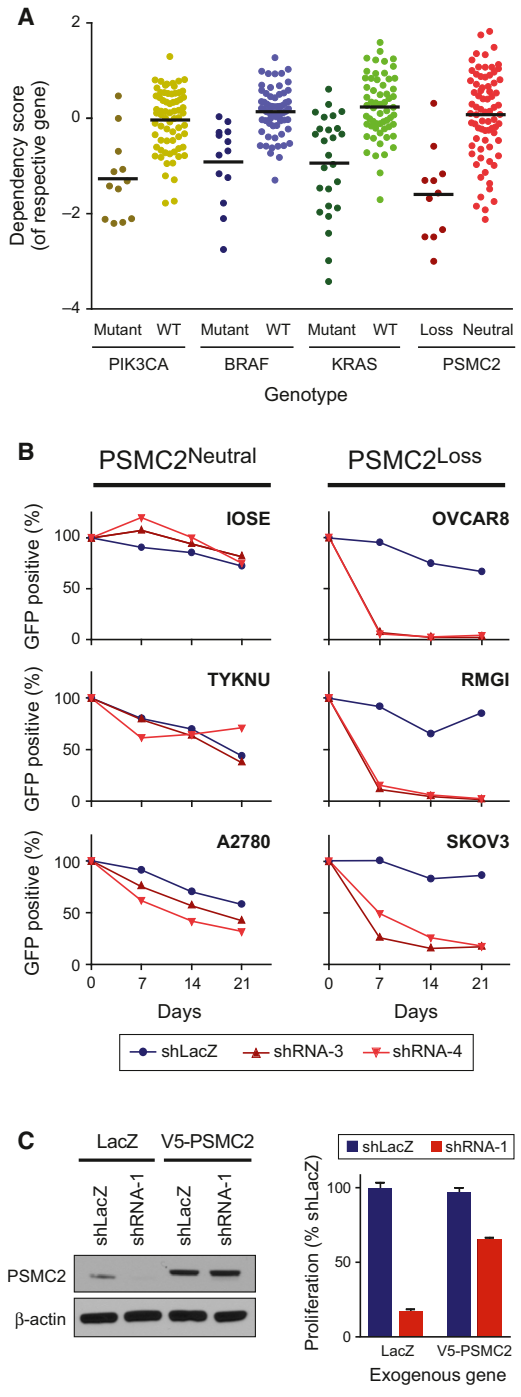

Figure 2. *PSMC2*^{Loss} Cells Are Sensitive to PSMC2 Suppression

(A) Comparison of gene dependence between three models of oncogene addiction and *PSMC2*. Cell lines were classified by mutation status for *PIK3CA*, *BRAF*, or *KRAS* (n = 102 in each case) or *PSMC2* copy number (n = 84). For each class, gene dependency scores reflect the sensitivity to the gene on which the categorization was based. Solid bars represent average scores.

(B) The effect of *PSMC2* suppression on the proliferation of six ovarian cell lines.

(C) PSMC2 levels (left) and relative proliferation rates (right) among cells expressing different combinations of *PSMC2* shRNA targeting the 3′ UTR and ectopic *V5-PSMC2* expression.

a *PSMC2*^{Loss} cell line. V5-PSMC2 expression was unaffected by an shRNA that targets the 3′ untranslated region (UTR) of endogenous *PSMC2* and rescued the proliferation of OVCAR8 cells that express this shRNA (Figure 2C). These observations confirmed that partial loss of *PSMC2* renders cancer cell lines highly dependent on the remaining *PSMC2*.

PSMC2 Levels and Survival in *PSMC2*^{Loss} Cell Lines

The increased vulnerability of *PSMC2*^{Loss} lines correlated with both *PSMC2* copy number loss and low mRNA expression (Table S4). Expression and copy number of *PSMC2* also correlate with each other in both the CCLE (r = 0.64) and TCGA ovarian (r = 0.49) sample sets (Figure S3A), indicating that cancer cells that have *PSMC2* copy number loss tolerate reduced *PSMC2* expression.

To explore the effects of *PSMC2* loss on PSMC2 protein levels, we evaluated PSMC2 levels in IOSE cells and in ten ovarian cancer cell lines, including five *PSMC2*^{Neutral} and five *PSMC2*^{Loss} lines. To minimize potential confounding of other genetic events affecting the 19S complex, we selected *PSMC2*^{Neutral} lines that had no copy number gains of *PSMC2* and *PSMC2*^{Loss} lines that had copy number loss of no more than one other 19S regulatory complex subunit (Table S6). All five *PSMC2*^{Loss} cell lines expressed lower levels of PSMC2 than any of the other cell lines (Figure 3A). In contrast, the levels of eight 19S subunits, including PSMC1 (Rpt2), PSMC4 (Rpt3), PSMC6 (Rpt4), PSMC3 (Rpt5), PSMC5 (Rpt6), PSMD2 (Rpn1), PSMD1 (Rpn2), and PSMD4 (Rpn10) or the 20S subunits PSMB5 (β5) and PSMA1–6 (α subunits) failed to correlate with *PSMC2* copy number (Figure S3B). Because PSMC2 is essential for cell proliferation, we concluded that *PSMC2*^{Neutral} cells either require more PSMC2 or produce more than is necessary for survival. Therefore, we engineered an experimental system to manipulate the levels of PSMC2 expression in both cell types.

Specifically, we expressed a *PSMC2*-specific shRNA under the control of a doxycycline-regulated promoter in *PSMC2*^{Loss} (Dox-shRNA-2 OVCAR8) and *PSMC2*^{Neutral} (Dox-shRNA-2 A2780) cells. The addition of doxycycline led to PMSC2 suppression in both cell lines (Figure 3B). Under these conditions, A2780 cells continued to proliferate, whereas OVCAR8 cells arrested in the G2 phase of the cell cycle and died by apoptosis (Figure S3C). To verify that A2780 cells tolerate increased *PSMC2* suppression, we varied the degree of suppression by modulating the doxycycline concentration. A 50% decrease in *PSMC2* mRNA reduced the proliferation of OVCAR8 cells, but not A2780 cells (Figure 3D), indicating that the *PSMC2*^{Neutral} line A2780 expresses more PSMC2 than is required for proliferation.

To determine the amount of PSMC2 required to maintain A2780 cell proliferation, we further suppressed PSMC2 expression by transfecting a pool of three *PSMC2*-specific siRNAs at varying concentrations. The proliferation of A2780 cells decreased only when *PSMC2* expression was suppressed by more than 60% (Figures S3D and S3E). By using quantitative RT-PCR and immunoblotting, we estimated that untreated

Data are presented as averages ±SD. See also Figure S2 and Tables S4 and S5.

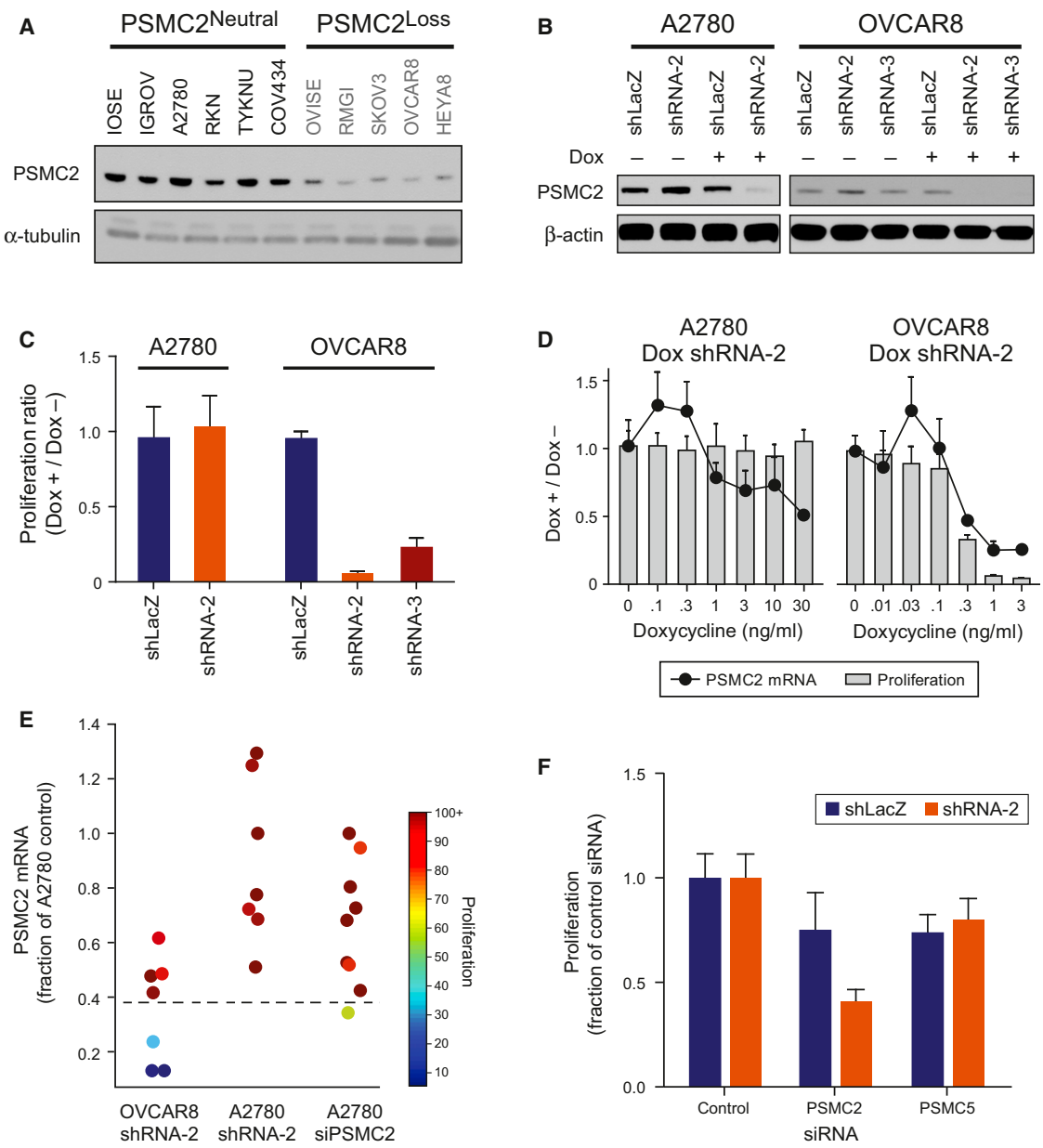

Figure 3. Threshold Requirement for PSMC2

(A) PSMC2 levels among ovarian cancer cell lines.

(B) PSMC2 levels in cells that express an inducible shRNA that targets either *PSMC2* or *LacZ*.

(C) Effects of *PSMC2* suppression on proliferation.

(D) Relationship between *PSMC2* mRNA expression and proliferation in *PSMC2*^{Neutral} (left) and *PSMC2*^{Loss} (right) cells. Data represent averages ±SD.

(E) Schematic combining data from Figures 3D, S3D, and S3E indicate that A2780 and OVCAR8 cells share a similar absolute threshold requirement for PSMC2 (dashed line).

(F) Cellular proliferation in A2780 cells with and without *PSMC2* suppression after introduction of control, *PSMC2*, or *PSMC5* siRNAs.

Data are presented as averages ±SEM. See also Figure S3 and Table S6.

OVCAR8 cells express ~50% of the *PSMC2* mRNA and protein found in A2780 cells (Figures S3F and S3G) and that both A2780 and OVCAR8 lose proliferative capacity at similar total levels of *PSMC2* expression (Figure 3E), suggesting that they have a comparable threshold requirement for *PSMC2*.

To determine whether partial loss of *PSMC2* affects the sensitivity of cells to suppression of other members of the 19S complex, we used an isogenic system in which Dox-shLacZ and Dox-shRNA-2 cells were cultured in doxycycline (30 ng/ml) so that shRNA-2 cells express levels of PSMC2 comparable to

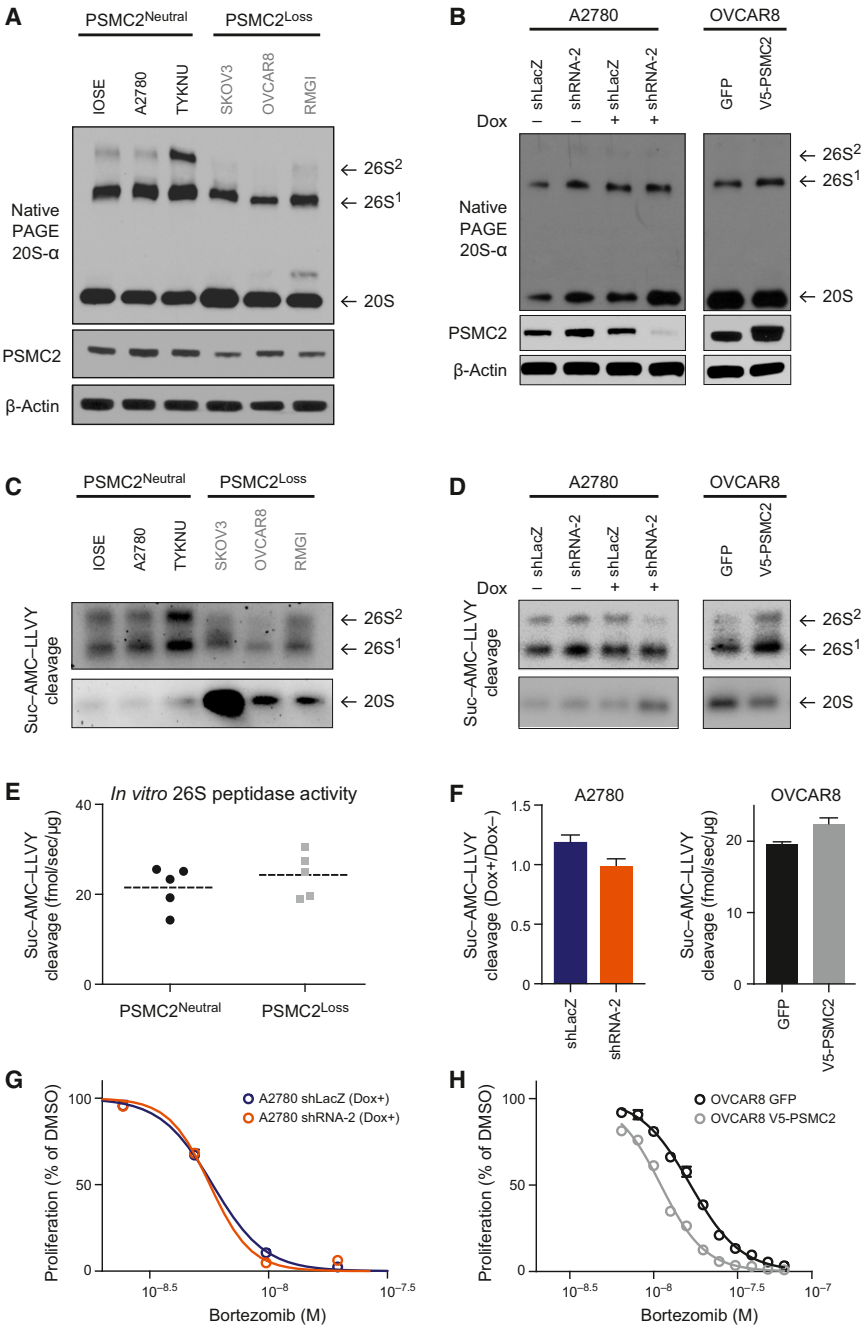

Figure 4. *PSMC2*^{Loss} Cells Lack a PSMC2 Reservoir

(A) Total PSMC2 levels (top) and native PAGE immunoblot for PSMA1–6 (middle) in *PSMC2*^{Neutral} and *PSMC2*^{Loss} cells.

(B) Native PAGE immunoblot for PSMA1–6 in A2780 (left) and OVCAR8 (right) after inducible suppression or ectopic expression of *PSMC2*, respectively.

(C) Native PAGE 26S and 20S peptidase cleavage in *PSMC2*^{Neutral} and *PSMC2*^{Loss} cells.

(D) Native PAGE 26S and 20S peptidase cleavage in isogenic systems used in (B).

(E) In vitro 26S proteasome activities in *PSMC2*^{Neutral} and *PSMC2*^{Loss} cells. Each point represents a cell line; dashed lines represent averages.

(F) In vitro 26S proteasome activities in isogenic systems used in (B) and (D).

(G and H) Dose response curve for bortezomib in (G) A2780 cells with and without *PSMC2* suppression and (H) OVCAR8 with and without ectopic V5-*PSMC2* expression.

See also Figure S4 and Table S7.

ure S3I). Together, these observations indicate that partial loss of *PSMC2* sensitizes cells to further suppression of *PSMC2*, but not of other 19S proteasome components.

PSMC2^{Loss} Cells Exhibit Only Slight Alterations in Proteasome Content and Function

The tolerance of cells for loss of *PSMC2* copy number and expression indicates that cells contain a reservoir of excess PSMC2 that is not required for proliferation. This reservoir may be maintained in an excess of fully assembled 26S proteasome or elsewhere in the cell. We analyzed proteasome assembly and content by performing PAGE on crude lysates under native (nondenaturing) conditions. Under these conditions, the 26S proteasome complex is stable and active and migrates in two distinct bands, which are distinguished by having either one or two 19S subunits incorporated in the formation of the 26S (Elsasser et al., 2005). By using lysates collected from IOSE, two *PSMC2*^{Neutral}, and three *PSMC2*^{Loss} cancer cell lines (all with comparable proliferation rates), we detected 26S^{1}, 26S^{2}, and 20S proteasome complexes by immunoblotting for the core 20S subunits, PSMA1–6 (Figure 4A).

We found that *PSMC2*^{Loss} lines express only slightly less 26S proteasome (most evident in 26S^{2}), which is not comparable to the decrease in PSMC2 in these cells (Figure 4A), and increased 20S proteasome. Similarly, comparable changes in PSMC2 expression in isogenic systems failed to substantially affect 26S

PSMC2^{Loss} cells. Under these conditions, both Dox-shLacZ and Dox-shRNA-2 proliferated at comparable rates. We then suppressed the expression of either *PSMC2* or *PSMC5* by introducing siRNA targeting these genes at concentrations that induce a similar degree of suppression of their intended target (Figure S3H). As expected, further suppression of *PSMC2* in Dox-shRNA-2 cells inhibited proliferation as compared to Dox-shLacZ cells (Figure 3F). In contrast, suppression of *PSMC5* led to a comparable inhibition of cell proliferation in both Dox-shLacZ and Dox-shRNA-2 cells. Suppression of *PSMC2* also did not affect the expression of other 19S components (Fig-

proteasome content. Suppression of *PSMC2* levels by 50% in the Dox-shRNA-2 A2780 system led to an increase in the 20S complex but little to no change in $26S^1$ (Figure 4B) or $26S^2$ (Figure S4A) proteasome content relative to controls. Conversely, ectopic expression of PSMC2 in OVCAR8 cells led to a slight reduction in 20S levels and slight increases in $26S^1$ and $26S^2$ proteasome content (Figures 4B and S4A). The levels of other 19S proteasome units remained unchanged (Figure S4B).

Similarly, peptidase cleavage activity varied only slightly between $PSMC2^{Neutral}$ and $PSMC2^{Loss}$ lines. We observed the greatest differences in in-gel analyses of peptidase activity, which revealed less $26S^2$ proteasome peptidase cleavage and increased 20S peptidase activity in $PSMC2^{Loss}$ cells (Figure 4C). These changes were recapitulated by *PSMC2* suppression in A2780 cells and were reversed by ectopic *PSMC2* expression in OVCAR8 cells (Figure 4D). The decrease in $26S^2$ activity in $PSMC2^{Loss}$ relative to $PSMC2^{Neutral}$ cells, however, was not associated with significant differences in peptidase cleavage when quantitatively assayed in whole-cell lysates under conditions (in the absence of SDS) in which free 20S proteasome does not contribute activity (Kisselev and Goldberg, 2005) ($p = 0.39$) (Figure 4E). In this assay, proteasome-specific peptidase activity is determined by bortezomib-inhibited cleavage. We found that 97% of activity was ablated by bortezomib, suggesting that other proteases did not contribute substantially to the measured activity. Lysates from $PSMC2^{Neutral}$ and $PSMC2^{Loss}$ lines grown under conventional nonstressed conditions also exhibited qualitatively similar total levels of polyubiquitin (Figure S4D).

To test the acute effect of manipulating PSMC2 expression on peptidase activity, we measured peptidase activity in lysates of A2780 cells in which we suppressed *PSMC2* and lysates of OVCAR8 cells engineered to recover *PSMC2* expression. Suppression of *PSMC2* by 50% in A2780 cells led to a 17% reduction in total 26S specific peptidase activity, which is associated with reduced $26S^2$ activity (Figure 4F). Conversely, ectopic *PSMC2* expression in OVCAR8 led to a 15% increase in peptidase activity, which is associated with increased $26S^2$ activity. The finding in both systems—that modulating PSMC2 levels by up to 50% resulted in only a 17% alteration in 26S activity—suggested that PSMC2 content was not the limiting component to 26S formation in $PSMC2^{Neutral}$ cells.

Across 133 cell lines previously tested, we found no increased sensitivity to bortezomib in $PSMC2^{Loss}$ cells and found no significant correlation between the concentration of bortezomib that inhibits proliferation by 50% (IC_{50}) and decreased expression of any of the 47 26S proteasome components (Garnett et al., 2012) (Table S7). Suppression of *PSMC2* in Dox-shRNA-2 A2780 cells or ectopic *PSMC2* expression in OVCAR8 cells also did not substantially affect the bortezomib IC_{50} (Figures 4G and 4H). These observations are consistent with our prior observation that 26S proteasome function is not substantially compromised in $PSMC2^{Loss}$ cells.

$PSMC2^{Neutral}$ Cells Have a Reservoir of PSMC2 that Buffers 26S Proteasome Levels against PSMC2 Loss

The finding that $PSMC2^{Neutral}$ cells have near-equal 26S proteasome content to $PSMC2^{Loss}$ cells, even though they express higher levels of PSMC2, suggests that $PSMC2^{Neutral}$ cells contain a separate reservoir of PSMC2 that is preferentially lost when levels are reduced. To identify this reservoir, we combined native PAGE with immunoblotting for PSMC2 across a panel of cell lines (Figure 5A). Of the multiple reactive bands identified, even after a long exposure, only one band ($Complex^{PSMC2}$) was present in all of the $PSMC2^{Neutral}$ lines, but none of the $PSMC2^{Loss}$ lines. By using isogenic systems, we also found that *PSMC2* suppression in Dox-shRNA-2 A2780 cells led to reduced levels of $Complex^{PSMC2}$, whereas ectopic PSMC2 expression in OVCAR8 cells led to its reappearance (Figure 5B). These results suggest that $Complex^{PSMC2}$ is a specific PSMC2 reservoir.

We hypothesized that $Complex^{PSMC2}$ serves as a "buffer" in $PSMC2^{Neutral}$ cells, enabling such cells to maintain 26S proteasome levels and function in the face of reduced PSMC2 expression. In this case, *PSMC2* suppression should deplete $Complex^{PSMC2}$ before reducing 26S proteasome levels. To quantify the consequences of reducing PSMC2 on $Complex^{PSMC2}$ and 26S proteasome levels, we compared dilutions of lysates from Dox shRNA-2 A2780 cells propagated in the absence of doxycycline to lysate collected from these cells cultured in doxycycline (Figure 5C). In cells in which *PSMC2* was suppressed, the relative loss of $Complex^{PSMC2}$ exceeded the decrease in 26S proteasome content. These observations indicate that $Complex^{PSMC2}$ was preferentially lost in A2780 cells after *PSMC2* suppression. In contrast, *PSMC2* suppression in OVCAR8 cells, which lack $Complex^{PSMC2}$, led to near-complete ablation of 26S proteasome levels and peptidase activity and led to a qualitative increase in the amount of polyubiquitin (Figures 5D–5F, S5A, and S5B).

To analyze the components of $Complex^{PSMC2}$, we fractionated lysates from IOSE cells expressing either V5-GFP or V5-PSMC2 (Figure S5C) by using a glycerol gradient (Figure S5D) and isolated V5-immune complexes containing either $Complex^{PSMC2}$ or 26S proteasome. $Complex^{PSMC2}$ immune complexes (collected in fractions 2–4) contained PSMC2, PSMC1 (Rpt2), PSMD2 (Rpn1), and PSMD5 (S5B) (Figure 5G), which are subunits of one of three complexes known to compose the base of the 19S proteasome (Funakoshi et al., 2009; Kaneko et al., 2009; Park et al., 2009; Roelofs et al., 2009; Saeki et al., 2009; Thompson et al., 2009). $Complex^{PSMC2}$ did not contain subunits of the other two complexes, PSMC3 (Rpt5), PSMC4 (Rpt3), PSMC5 (Rpt6), and PSMC6 (Rpt4), or members of the 20S proteasome, PSMB5 (β5) or PSMA1–6 (α subunits) (Figure 6C). All of these proteins, except PSMD5, were detected in immune complexes containing the 26S complex (from fractions 7–9). These observations indicate that the PSMC2 reservoir is a subcomplex of the 26S proteasome.

The Reduction of PSMC2 Levels in $PSMC2^{Loss}$ Cells Inhibits Orthotopic Tumor Growth

To explore the therapeutic potential of *PSMC2* suppression in vivo, we tested the consequences of suppressing *PSMC2* in ovarian xenografts. Specifically, we used a tumor-targeted nanoparticle delivery system that delivers small interfering RNA (siRNA) into the cytosol of cells within the tumor parenchyma (Ren et al., 2012). We generated tumor-penetrating

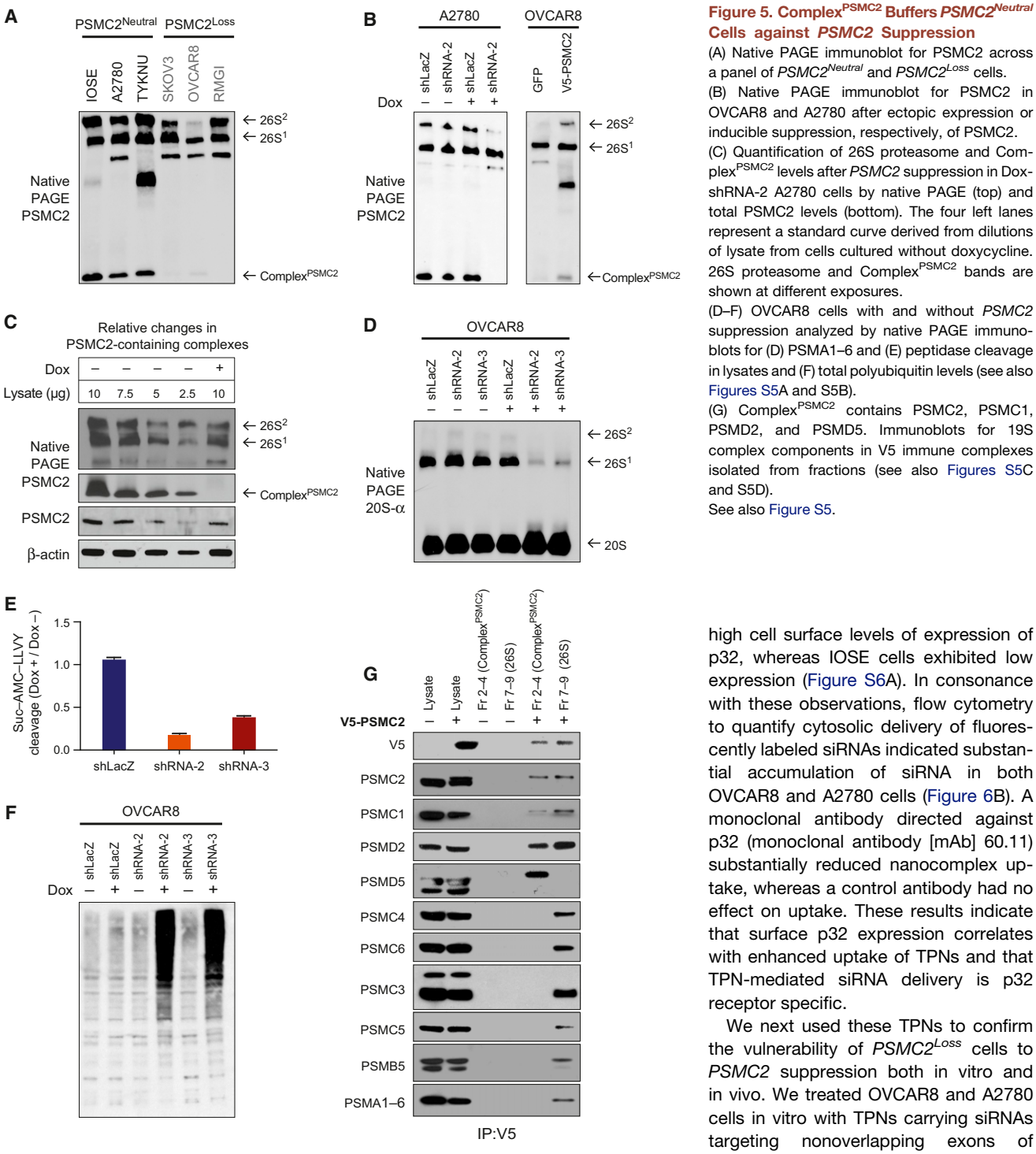

Figure 5. Complex^{PSMC2} Buffers *PSMC2*^{Neutral} Cells against *PSMC2* Suppression

(A) Native PAGE immunoblot for PSMC2 across a panel of *PSMC2*^{Neutral} and *PSMC2*^{Loss} cells.

(B) Native PAGE immunoblot for PSMC2 in OVCAR8 and A2780 after ectopic expression or inducible suppression, respectively, of PSMC2.

(C) Quantification of 26S proteasome and Complex^{PSMC2} levels after *PSMC2* suppression in Dox-shRNA-2 A2780 cells by native PAGE (top) and total PSMC2 levels (bottom). The four left lanes represent a standard curve derived from dilutions of lysate from cells cultured without doxycycline. 26S proteasome and Complex^{PSMC2} bands are shown at different exposures.

(D–F) OVCAR8 cells with and without *PSMC2* suppression analyzed by native PAGE immunoblots for (D) PSMA1–6 and (E) peptidase cleavage in lysates and (F) total polyubiquitin levels (see also Figures S5A and S5B).

(G) Complex^{PSMC2} contains PSMC2, PSMC1, PSMD2, and PSMD5. Immunoblots for 19S complex components in V5 immune complexes isolated from fractions (see also Figures S5C and S5D).

See also Figure S5.

nanocomplexes (TPNs) consisting of *PSMC2*-specific siRNA noncovalently bound to tandem peptides bearing an N-terminal cell-penetrating domain, Transportan (TP), and a C-terminal tumor-specific domain, LyP-1 (CGNKRTRGC), which binds to its cognate receptor p32 (Figure 6A).

We first assessed the compatibility of cell lines with TPN-targeted siRNA delivery. OVCAR8 and A2780 cells exhibited high cell surface levels of expression of p32, whereas IOSE cells exhibited low expression (Figure S6A). In consonance with these observations, flow cytometry to quantify cytosolic delivery of fluorescently labeled siRNAs indicated substantial accumulation of siRNA in both OVCAR8 and A2780 cells (Figure 6B). A monoclonal antibody directed against p32 (monoclonal antibody [mAb] 60.11) substantially reduced nanocomplex uptake, whereas a control antibody had no effect on uptake. These results indicate that surface p32 expression correlates with enhanced uptake of TPNs and that TPN-mediated siRNA delivery is p32 receptor specific.

We next used these TPNs to confirm the vulnerability of *PSMC2*^{Loss} cells to *PSMC2* suppression both in vitro and in vivo. We treated OVCAR8 and A2780 cells in vitro with TPNs carrying siRNAs targeting nonoverlapping exons of *PSMC2*. In both cell types, we observed a reduction of PSMC2 protein relative to cells treated with TPNs carrying *GFP* siRNA (Figure S6B). This reduction was associated with a corresponding decrease in proliferation only in the OVCAR8 cells (Figure S6C). We then used these TPNs to treat mice harboring orthotopic OVCAR8 or A2780 tumors expressing firefly luciferase. We injected TPNs carrying *PSMC2*-siRNA (1 mg siRNA/kg body weight for 14 days) intraperitoneally

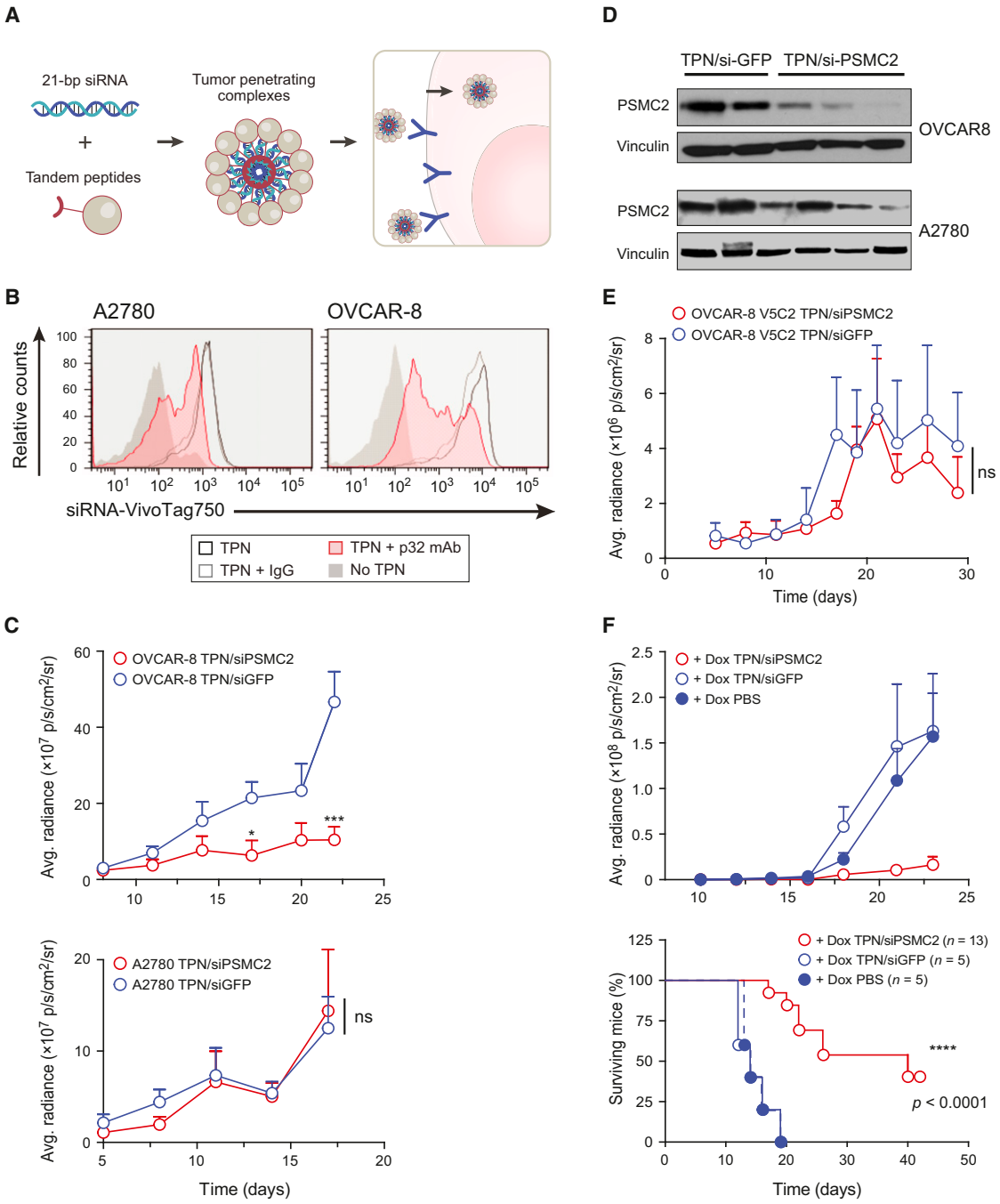

Figure 6. Tumor-Penetrating Nanocomplex-Mediated Delivery of *PSMC2*-Specific siRNA Suppresses Ovarian Tumor Growth

(A) Schematic depicting the mechanism of TPN-mediated delivery of siRNA.

(B) Comparison of cellular uptake of fluorescently labeled siRNA in untreated cells (solid gray) and cells treated with TPN alone (black line) and in combination with IgG (gray line) or an antibody to p32 (solid pink).

(C) Tumor burden of mice bearing disseminated OVCAR8 (top) or A2780 (bottom) orthotopic xenografts treated with TPN carrying either GFP-siRNA or *PSMC2*-siRNA. n = 5 animals per group.

(D) PSMC2 levels in orthotopic tumors of A2780 or OVCAR8 after treatment with nanoparticles carrying siGFP or siPSMC2.

(E) Tumor burden of mice bearing orthotopic tumors of OVCAR8 cells expressing *V5-PSMC2*. n = 5 animals per group.

(F) Tumor burden (top) and overall survival (bottom) of mice bearing orthotopic tumors of A2780 cells expressing doxycycline-inducible shRNA against *PSMC2*. n = 5–13 animals per group.

Data in all panels are presented as average ±SEM. Significance was determined by one-way analysis of variance (ANOVA) or log rank (Mantel-Cox) tests as appropriate. n.s., not significant; *p < 0.05; **p < 0.01; ***p < 0.001; ****p < 0.0001. See also Figure S6.

every 3 days and monitored tumor burden noninvasively by imaging bioluminescence. We observed a reduction in tumor burden (by >75% relative to tumors treated with siGFP) only in OVCAR8 tumors (Figure 6D). A2780 and any remaining OVCAR8 tumors treated with TPN/siPSMC2 exhibited lower levels of PSMC2, but not two other members of Complex^{PSMC2}, PSMC1 and PSMD5 (Figures 6D and S6D).

However, TPN/siPSMC2 nanoparticles failed to decrease tumor burden of *PSMC2*^{Loss} cells in which we reconstituted PSMC2 expression in vivo by using orthotopic tumor xenografts derived from OVCAR8 cells expressing V5-PSMC2 (Figure 6E). This finding confirmed that the effects of TPN/siPSMC2 on tumor growth were the consequence of reduced PSMC2 expression.

Conversely, TPN/siPSMC2 nanoparticles reduced tumor growth and significantly improved survival in *PSMC2*^{Neutral} cells expressing *PSMC2*-specific shRNAs (Figure 6F). We measured the effects of TPN/siPSMC2 nanoparticles relative to TPN/siGFP or PBS in mice with xenografts of A2780 cells engineered to express inducible *PSMC2* shRNA. Among mice treated with doxycycline and TPN/siPSMC2, overall survival was 40 days, and 40% survived more than 42 days, whereas all animals in the TPN/siGFP and PBS cohorts succumbed to tumors within 19 days ($p = 0.0013$) (Figure 6F). These findings demonstrated the therapeutic efficacy of *PSMC2* suppression in vivo and support the notion that *PSMC2*^{Loss} cells are sensitive to suppression of *PSMC2* due to decreased basal levels of *PSMC2* mRNA.

DISCUSSION

PSMC2 as a CYCLOPS Gene

By integrating data derived from the genomic characterization of human tumors with systematic interrogation of essential genes in cancer cell lines, we have identified a distinct class of cancer-specific vulnerabilities associated with partial copy number loss of essential genes. Hemizygous loss of *PSMC2* in particular and of CYCLOPS genes in general renders cells highly dependent on the remaining allele. Although *PSMC2* is frequently involved in partial copy number loss, we did not observe homozygous deletion, which is consistent with the notion that *PSMC2* is an essential gene. Partial copy number loss, in contrast, did not substantially impact either proteasome function or cell proliferation.

26S proteasome components are not in stoichiometric equilibrium, and the limiting components may differ between cancer and normal cells. For example, cells often express free 20S complex, but not 19S, suggesting that 26S proteasome levels are limited by 19S regulatory complex levels (Figure 4A). The modules that make up the base of the 19S complex may be similarly imbalanced. We found that the module containing PSMC2 (Rpt1), PSMC1 (Rpt2), PSMD2 (Rpn1), and PSMD5 (S5B) was in excess in many cancer cell lines, yet it became limiting to 19S formation in *PSMC2*^{Loss} cells, unveiling a new sensitivity. PSMC2 levels are influenced by its subcomplex partners (Kaneko et al., 2009), suggesting that interfering with the formation of Complex^{PSMC2} or with its incorporation into the 19S proteasome may be a specific approach to reduce PSMC2 levels and proliferation of *PSMC2*^{Loss} cells. Indeed, when we suppressed *PSMC2* in vivo, we were able to obtain more than 75% reductions in tumor burden and a doubling of overall survival.

Because the proteasome is essential in all cells, one concern is whether targeting PSMC2 would induce substantial toxicity in noncancer cells. However, proteasome inhibition has been well tolerated in humans. Although bortezomib treatment results in a 70% reduction of proteasome-specific peptidase cleavage, it is well tolerated with acceptable side effect profiles. (Aghajanian et al., 2002). In comparison, proliferation of *PSMC2*^{Loss} cells is reduced at levels of *PSMC2* suppression that result in only a 15% reduction of peptide cleavage in *PSMC2*^{Neutral} cells.

More generally, our findings suggest that one consequence of genomic instability is an alteration in the stoichiometry of components of macromolecular machines, including the proteasome, ribosome, and spliceosome. These observations suggest that many of these imbalances may present potential therapeutic targets in individual components or precursor complexes and that these components, rather than the fully assembled machines, will require specific inhibition or disruption.

CYCLOPS Genes as Synthetic Lethal Targets

CYCLOPS genes represent a specific form of synthetic lethality. Several studies have investigated synthetic lethality with activation of pathways that drive cancer but that cannot themselves be easily targeted. For example, synthetic lethality is one approach to targeting inactivated tumor suppressor genes, whose functions cannot easily be reconstituted. Recent observations—that breast and ovarian cancers that harbor *BRCA1* or *BRCA2* loss and impaired homologous recombination DNA repair pathway are highly dependent on the nucleotide excision DNA repair pathway (Bryant et al., 2005; Farmer et al., 2005)—provide evidence that synthetic lethality may be clinically useful. Targeting CYCLOPS genes represents a different approach to synthetic lethality. In this case, the intervention is lethal to cells with a genetic event that is independent of that event's effect on the pathways that drive cancer.

Discovery of New Vulnerabilities due to Genomic Disruption in Cancer

Advances in cancer therapeutics benefit from our ability to identify vulnerabilities predicted by genomic features that are unique to cancer cells. Indeed, the inhibition of recurrent activating mutations in proto-oncogenes has led to several new cancer treatments. The cancer-specific vulnerabilities we have identified herein are the consequence of alterations in genes affected by genomic disruption that may have no consequence to the process by which the cell transformed or continues to proliferate. These genomic alterations are more frequent than most known driver alterations, occur across lineages, and could theoretically be targeted in a large number of patients.

Although individual CYCLOPS candidates such as *PSMC2* will require further investigation in human subjects, the 56 candidate genes we identified may be an underestimate of the true number of potential targets. Our initial Project Achilles analysis included only 5,312 genes, and many of these genes may represent false negative results due to insufficiently effective shRNAs. The set of 86 cell lines was not large enough to enable detection of lineage-specific CYCLOPS genes. Indeed, we identified additional

CYCLOPS targets in an independently generated RNAi data set enriched in breast and pancreatic lineages, in addition to validating the targets described in our more lineage-diverse data set. Systematic evaluation of the completely annotated genome using more shRNAs for each gene and a larger group of cell lines representing many lineages is likely to uncover many more potential targets.

Besides copy number loss, other types of genomic alteration may also unveil CYCLOPS vulnerabilities. In most cases, vulnerability to suppression of CYCLOPS genes was associated with decreased expression. Other events may also decrease expression of essential genes, including sequence variants, epigenetic modification, or chromosome translocations. Any of these mechanisms may lead to cancer-specific vulnerabilities. Further work will be necessary to explore these other classes and to define the role of CYCLOPS targets in cancer therapy.

EXPERIMENTAL PROCEDURES

Copy Number and Methylation Analysis of Tumors

Copy numbers were determined for 3,131 cancer samples as previously described (Mermel et al., 2011). Marker and gene locations were based on the hg18 genome build. The criteria used to define partial copy number loss, homozygous deletion, and the length of each deletion are detailed in the Extended Experimental Procedures. Gene-level DNA methylation β values were collected for 601 ovarian tumors from the TCGA web portal. Genes with β values >0.7 were considered methylated. Genes missing data in any sample were excluded from the analysis.

CYCLOPS Analysis

For each cell line, we classified each gene as intact (no copy number loss) or partial loss or to be excluded (for genes undergoing homozygous loss or with ambiguous data) based on thresholds determined by using the distribution of relative copy numbers generated from analysis of SNP array data for that cell line (see Extended Experimental Procedures). Gene dependency scores were determined by using the ATARiS algorithm (see Extended Experimental Procedures). The statistical significance of mean gene dependency score differences between intact and partial loss cell lines was determined by comparing the observed data to data representing 50,000 random permutations of class labels, each maintaining the number of cell lines and lineage distribution in each class. Multiple hypotheses were corrected by using the FDR framework (Benjamini and Hochberg, 1995).

26S Proteasome Activity

We measured excitation-emission spectra (360 nm to 430 nm) during incubation in vitro at 37°C every 30 s for 1 hr for a 100 μl solution containing 5 μl of lysate (buffer A) in 50 mM Tris-HCl (pH 8.0), 40 mM KCl, 5 mM $MgCl_2$, 1 mM ATP, 1 mM dithiothreitol (DTT), and 100 μM Sucrose-LLVY-AMC (Bachem). We converted these measurements to amount of peptide cleavage by using a standard curve generated from the excitation-emission spectra of AMC (Bachem). Samples were tested in triplicate with and without the addition of 1 μM bortezomib. The average value of peptide cleavage in the bortezomib sample was subtracted to determine 26S proteasome activity. The reagents used in this assay and the procedure to make lysates are described in the Extended Experimental Procedures.

Native Gel Analysis for Proteasome Content or Proteasome Activity

10 μg of lysate (buffer A) was loaded onto 3%–8% Tris-Acetate PAGE (Invitrogen) and run in Tris-Glycine at 4°C and 60V for 17 hr. Gels were transferred to nitrocellulose membranes in Tris-Glycine at 70V for 4 hr for immunoblotting or in-gel peptidase activity. The latter was performed by incubating with gentle agitation in 50 mM Tris-HCl (pH 8.0), 5 mM $MgCl_2$, 1 mM ATP, 1 mM DTT, and 50 μM Suc-LLVY-AMC (Bachem) at 37°C for 30 min. Gels were visualized under UV transillumination. Following photography of 26S proteasome activity, gels were incubated for another 45 min at 37°C in the same buffer with the addition of 0.2% SDS and reanalyzed by UV transillumination to assess 20S peptidase activity.

Generation of PSMC2-Specific and Control siRNA Nanoparticles

The generation of TPN carrying PSMC2-siRNA (Dharmacon) and measurement of their uptake and effects on proliferation were performed as described (Ren et al., 2012). The p32-receptor specificity of cell uptake was probed by using a monoclonal antibody directed against p32 (100 μg/ml) to cells 1 hr prior to the addition of TPN. More information about the reagents, chemicals, and siRNA sequences can be found in the Extended Experimental Procedures.

Generation of Orthotopic Xenografts and TPN Administration

10^6 OVCAR8 cells, 0.5 × 10^6 OVCAR8 cells expressing V5-PSMC2, or 0.2 × 10^6 A2780 cells expressing doxycycline-inducible shRNA against *PSMC2* were implanted intraperitoneally in 4- to 6-week-old NCr/nude mice (Charles River). Once tumors were established and confirmed by bioluminescence imaging, animals were treated intraperitoneally with nanoparticles carrying *GFP*-specific siRNA (TPN/siGFP) or with TPN containing *PSMC2*-specific siRNA (1 mg siRNA/kg/injection) every 3 days for 21 days, as described (Ren et al., 2012). Mice bearing A2780 tumors expressing the doxycycline-inducible sh*PSMC2* were continuously fed with doxycycline-containing diet (2,000 mg/kg) beginning 2 days after tumor cell injection. Mice were sacrificed, and tumors were harvested at the end of the experiment or when the tumor burden resulted in a failure to thrive according to institutional recommendations. Tumor lysates were made by homogenizing tumors using an Eppendorf micropestle in RIPA buffer supplemented with protease inhibitors.

SUPPLEMENTAL INFORMATION

Supplemental Information includes Extended Experimental Procedures, six figures, and seven tables and can be found with this article online at http://dx.doi.org/10.1016/j.cell.2012.07.023.

ACKNOWLEDGMENTS

We would like to thank Leslie Gaffney and Lauren Solomon for support in generating illustrations and graphics and Jesse Boehm, Scott Carter, George Demartino, and members of the Goldberg and Hahn lab for helpful discussion. This work was supported in part by NIH/NCI grants RC2 CA148268 (W.C.H.), U54 CA143798, K08 CA122833 (R.B.), T32 GM008313 (T.I.Z.), RO1 GM051923-17 (A.L.G and H.C.B.), and U54 CA112962 (A.T., J.P.M., W.C.H.), the H.L. Snyder Medical Foundation (W.C.H.), the V Foundation (R.B.), a Conquer Cancer Foundation Young Investigator Award (D.N.), Sass Foundation Fellowship (D.N.), and the Marie D. & Pierre Casimir-Lambert Fund. S.N.B. is a Howard Hughes Investigator. W.C.H. and R.B. are consultants for Novartis Pharmaceuticals.

Received: May 27, 2012
Revised: July 21, 2012
Accepted: July 26, 2012
Published online: August 15, 2012

REFERENCES

Aghajanian, C., Soignet, S., Dizon, D.S., Pien, C.S., Adams, J., Elliott, P.J., Sabbatini, P., Miller, V., Hensley, M.L., Pezzulli, S., et al. (2002). A phase I trial of the novel proteasome inhibitor PS341 in advanced solid tumor malignancies. Clin. Cancer Res. *8*, 2505–2511.

Ashworth, A., Lord, C.J., and Reis-Filho, J.S. (2011). Genetic interactions in cancer progression and treatment. Cell *145*, 30–38.

Barretina, J., Caponigro, G., Stransky, N., Venkatesan, K., Margolin, A.A., Kim, S., Wilson, C.J., Lehár, J., Kryukov, G.V., Sonkin, D., et al. (2012). The Cancer

Cell Line Encyclopedia enables predictive modelling of anticancer drug sensitivity. Nature *483*, 603–607.

Benjamini, Y., and Hochberg, Y. (1995). Controlling the false discovery rate: a practical and powerful approach to multiple testing. J. R. Stat. Soc. Ser. B Methodol. *57*, 289–300.

Beroukhim, R., Mermel, C.H., Porter, D., Wei, G., Raychaudhuri, S., Donovan, J., Barretina, J., Boehm, J.S., Dobson, J., Urashima, M., et al. (2010). The landscape of somatic copy-number alteration across human cancers. Nature *463*, 899–905.

Brose, M.S., Volpe, P., Feldman, M., Kumar, M., Rishi, I., Gerrero, R., Einhorn, E., Herlyn, M., Minna, J., Nicholson, A., et al. (2002). BRAF and RAS mutations in human lung cancer and melanoma. Cancer Res. *62*, 6997–7000.

Bryant, H.E., Schultz, N., Thomas, H.D., Parker, K.M., Flower, D., Lopez, E., Kyle, S., Meuth, M., Curtin, N.J., and Helleday, T. (2005). Specific killing of BRCA2-deficient tumours with inhibitors of poly(ADP-ribose) polymerase. Nature *434*, 913–917.

Cancer Genome Atlas Research Network. (2011). Integrated genomic analyses of ovarian carcinoma. Nature *474*, 609–615.

Cheung, H.W., Cowley, G.S., Weir, B.A., Boehm, J.S., Rusin, S., Scott, J.A., East, A., Ali, L.D., Lizotte, P.H., Wong, T.C., et al. (2011). Systematic investigation of genetic vulnerabilities across cancer cell lines reveals lineage-specific dependencies in ovarian cancer. Proc. Natl. Acad. Sci. USA *108*, 12372–12377.

Daley, G.Q., Vanetten, R.A., and Baltimore, D. (1990). Induction of chronic myelogenous leukemia in mice by the P210BCR/ABL gene of the Philadelphia chromosome. Science *247*, 824–830.

Elsasser, S., Schmidt, M., and Finley, D. (2005). Characterization of the proteasome using native gel electrophoresis. Methods Enzymol. *398*, 353–363.

Farmer, H., McCabe, N., Lord, C.J., Tutt, A.N., Johnson, D.A., Richardson, T.B., Santarosa, M., Dillon, K.J., Hickson, I., Knights, C., et al. (2005). Targeting the DNA repair defect in BRCA mutant cells as a therapeutic strategy. Nature *434*, 917–921.

Finley, D. (2009). Recognition and processing of ubiquitin-protein conjugates by the proteasome. Annu. Rev. Biochem. *78*, 477–513.

Frei, E., III. (1993). Gene deletion: a new target for cancer-chemotherapy. Lancet *342*, 662–664.

Funakoshi, M., Tomko, R.J., Jr., Kobayashi, H., and Hochstrasser, M. (2009). Multiple assembly chaperones govern biogenesis of the proteasome regulatory particle base. Cell *137*, 887–899.

Garnett, M.J., Edelman, E.J., Heidorn, S.J., Greenman, C.D., Dastur, A., Lau, K.W., Greninger, P., Thompson, I.R., Luo, X., Soares, J., et al. (2012). Systematic identification of genomic markers of drug sensitivity in cancer cells. Nature *483*, 570–575.

Kaelin, W.G., Jr. (2005). The concept of synthetic lethality in the context of anticancer therapy. Nat. Rev. Cancer *5*, 689–698.

Kaneko, T., Hamazaki, J., Iemura, S., Sasaki, K., Furuyama, K., Natsume, T., Tanaka, K., and Murata, S. (2009). Assembly pathway of the mammalian proteasome base subcomplex is mediated by multiple specific chaperones. Cell *137*, 914–925.

Kisselev, A.F., and Goldberg, A.L. (2005). Monitoring activity and inhibition of 26S proteasomes with fluorogenic peptide substrates. Methods Enzymol. *398*, 364–378.

Liu, J., Yang, G., Thompson-Lanza, J.A., Glassman, A., Hayes, K., Patterson, A., Marquez, R.T., Auersperg, N., Yu, Y., Hahn, W.C., et al. (2004). A genetically defined model for human ovarian cancer. Cancer Res. *64*, 1655–1663.

Marcotte, R., Brown, K.R., Suarez, F., Sayad, A., Karamboulas, K., Krzyzanowski, P.M., Sircoulomb, F., Medrano, M., Fedyshyn, Y., Koh, J.L.Y., et al. (2012). Essential gene profiles in breast, pancreatic, and ovarian cancer cells. Cancer Discov. *2*, 172–189.

Mermel, C.H., Schumacher, S.E., Hill, B., Meyerson, M.L., Beroukhim, R., and Getz, G. (2011). GISTIC2.0 facilitates sensitive and confident localization of the targets of focal somatic copy-number alteration in human cancers. Genome Biol. *12*, R41.

Park, S., Roelofs, J., Kim, W., Robert, J., Schmidt, M., Gygi, S.P., and Finley, D. (2009). Hexameric assembly of the proteasomal ATPases is templated through their C termini. Nature *459*, 866–870.

Ren, Y., Cheung, H.W., von Maltzhan, G., Agrawal, A., Cowley, G.S., Weir, B.A., Boehm, J.S., Tamayo, P., Karst, A.M., Liu, J.F., et al. (2012). Targeted tumor-penetrating siRNA nanocomplexes for credentialing the ovarian cancer target ID4. Sci. Transl. Med. *4*, 147ra112.

Richardson, P.G., Sonneveld, P., Schuster, M.W., Irwin, D., Stadtmauer, E.A., Facon, T., Harousseau, J.L., Ben-Yehuda, D., Lonial, S., Goldschmidt, H., et al; Assessment of Proteasome Inhibition for Extending Remissions (APEX) Investigators. (2005). Bortezomib or high-dose dexamethasone for relapsed multiple myeloma. N. Engl. J. Med. *352*, 2487–2498.

Roelofs, J., Park, S., Haas, W., Tian, G., McAllister, F.E., Huo, Y., Lee, B.H., Zhang, F., Shi, Y.G., Gygi, S.P., and Finley, D. (2009). Chaperone-mediated pathway of proteasome regulatory particle assembly. Nature *459*, 861–865.

Saeki, Y., Toh-E, A., Kudo, T., Kawamura, H., and Tanaka, K. (2009). Multiple proteasome-interacting proteins assist the assembly of the yeast 19S regulatory particle. Cell *137*, 900–913.

Sawyers, C.L. (2005). Making progress through molecular attacks on cancer. Cold Spring Harb. Symp. Quant. Biol. *70*, 479–482.

Smith, D.M., Fraga, H., Reis, C., Kafri, G., and Goldberg, A.L. (2011). ATP binds to proteasomal ATPases in pairs with distinct functional effects, implying an ordered reaction cycle. Cell *144*, 526–538.

Soda, M., Choi, Y.L., Enomoto, M., Takada, S., Yamashita, Y., Ishikawa, S., Fujiwara, S.I., Watanabe, H., Kurashina, K., Hatanaka, H., et al. (2007). Identification of the transforming EML4-ALK fusion gene in non-small-cell lung cancer. Nature *448*, 561–566.

Solimini, N.L., Luo, J., and Elledge, S.J. (2007). Non-oncogene addiction and the stress phenotype of cancer cells. Cell *130*, 986–988.

Stratton, M.R., Campbell, P.J., and Futreal, P.A. (2009). The cancer genome. Nature *458*, 719–724.

Thompson, D., Hakala, K., and DeMartino, G.N. (2009). Subcomplexes of PA700, the 19 S regulator of the 26 S proteasome, reveal relative roles of AAA subunits in 26 S proteasome assembly and activation and ATPase activity. J. Biol. Chem. *284*, 24891–24903.

Weinstein, I.B., and Joe, A.K. (2006). Mechanisms of disease: Oncogene addiction—a rationale for molecular targeting in cancer therapy. Nat. Clin. Pract. Oncol. *3*, 448–457.

Zhang, R., and Lin, Y. (2009). DEG 5.0, a database of essential genes in both prokaryotes and eukaryotes. Nucleic Acids Res. *37*(Database issue), D455–D458.

EXTENDED EXPERIMENTAL PROCEDURES

Copy Number Analysis of Tumor Samples

Using copy number data collected from 3,131 cancer samples, we considered markers with relative $\log_2$ copy number ratios less than -0.1 to be affected by partial copy number loss, and markers less than -1.28 as homozygous deletions (Beroukhim et al., 2010). Copy number profiles, and the locations, lengths, and amplitudes of the amplification and deletion events underlying these profiles, were determined as previously described (Mermel et al., 2011). We determined whether the difference in rates of homozygous loss, hemizygous loss, or DNA methylation were significant between CYCLOPS and non-CYCLOPS genes by comparing the observed rate of the respective copy number change to the rate after permutation of gene names.

Copy Number Analysis of Cancer Cell Lines from CCLE

For each sample, we created a 100 bin histogram of copy number values for all markers, and then used a 5-bin moving average to smooth this distribution. This procedure typically yielded 2-5 well-separated peaks (local maxima with height as measured from local max to surrounding local minima > 2% of genome), presumably corresponding to integer level copy loss and gains. Based on these peaks, samples were separated into one of two categories for classification. If a sample contained one peak between $\log_2$ copy number -0.05 and 0.05, with a second peak between -0.05 and -0.4, the first peak was defined as copy neutral, and the second peak as partial copy loss. In this case, the cutoff for copy loss was set at 95% upper bound of the second peak, and the cutoff for copy neutral was set at 95% lower bound of the first peak. If there were no peak that met our height criteria within these regions in a given sample, markers < -0.4 were considered copy loss, whereas markers > -0.2 were considered copy neutral. In either case, markers that lay between our two cutoffs were left uncalled and genes with these copy numbers were excluded from further analysis. Markers with $\log_2$ copy number ratios ≤ -1.28 were considered homozygous loss and genes with these copy numbers were also removed from further analyses. We used the Kolmogorov-Smirnov test to determine enrichment of the CYCLOPs genes identified in our original analysis among the most significant genes in our analysis of the Validation data set.

Analysis of Copy Number and Expression Correlations

Quantized normalized expression data were obtained from the CCLE (www.broadinstitute.org/ccle) and TCGA (https://tcga-data.nci.nih.gov/tcga/) portals. Enrichment of Pearson correlation coefficients among CYCLOPS candidates and pathways was determined by permuting gene names. A similar analysis was used to determine significance of correlation between bortezomib log IC_{50} values for 133 cancer cell lines collected from Sanger center Cancer Genome Project (http://www.sanger.ac.uk/genetics/CGP/) portal and the expression patterns for these lines from the CCLE (www.broadinstitute.org/ccle).

Analysis to Determine Correlation between Gene Dependence Scores and mRNA Expression

We used the ATARiS algorithm (A.T., W.C.H., and J.P.M., unpublished data) to determine gene dependencies for individual cell lines using only shRNAs that have similar effects across cell lines. ATARiS assesses gene suppression effects in each sample of multi-sample RNAi screens that include at least two RNAi reagents (siRNA or shRNA) designed to target each gene. For each gene, ATARiS generates a quantitative gene dependency score that summarizes the results of the subset of reagents targeting the gene that induce similar effects across all screened samples, under the assumption that these effects are likely due to on-target rather than off-target gene suppression. These gene dependency scores represent the determined relative level of dependency of each sample on the expression of each screened gene. In some cases, a gene may have multiple solutions based on a different subset of its shRNAs. ATARIS determined 8,280 gene dependency scores for 7,250 genes in the Achilles data set.

Competition Assays Using shRNA Constructs

We found that a single lentiviral integrant expressing either shRNA-1 or shRNA-3 was sufficient to suppress PSMC2 levels in *PSMC2*^{Neutral} cells relative to cells that express shLacZ (Figure S2B); competition assays were therefore performed at a multiplicity of infection of 1. To perform competition assays, *PSMC2* shRNA-3, *PSMC2* shRNA-4, and *PSMC2* shLacZ in pLKO.1 were modified by inserting *GFP* into the puromycin cassette (BamHI/Kpn1) to yield pLKO GFP constructs that expressed these shRNAs. Cells were infected with lentivirus that contained the indicated shRNA in pLKO.1 GFP and treated for 24 hr with three fold dilutions of virus according to protocols for lentiviral infection. At 48 hr, the cells were analyzed using a BD LSR II flow cytometry system (BD Biosciences) for GFP+ cells. The well in which the viral titer resulted in approximately 50% of GFP+ cells was then cultured for 21 d. Using FACS, we analyzed these cell populations for GFP+ cells on days 7, 14, and 21 and recorded the percentage of GFP+ cells normalized to the day 0 time point.

Reagents

The following antibodies were used: PSMC2 (Enzo, PW8825), PSMC1 (Enzo, PW8305), PSMC3 (Enzo, PW8770), PSMC4 (Enzo, PW8175), PSMC5 (Enzo, PW8770), PSMD5 (Thermo Fisher, PA1975), PSMD2 (Proteintech, 14748-1-AP), PSMD11 (Enzo, PW8370), β-Actin (Santa Cruz, C4), Vinculin (Sigma, V9131), Ubiquitin (Santa Cruz, P4D1), PSMB5 (Proteintech, 19178-1-AP), PSMD1 (Enzo, PW9270), PSMA1–6 (Enzo, PW8195), PSMD4 (Enzo, PW9250), GAPDH (Cell Signaling), Anti-V5/HRP (Invitrogen), p32 (Millipore - mAb 60.11).

Lentiviral vectors expressing shRNAs were obtained from The RNAi Consortium (TRC) at the Broad Institute in pLKO.1 (http://www.broadinstitute.org/rnai/public). The shRNA, target gene, target sequence, and TRC number are as follows: *PSMC2* shRNA-1, 5′ CCTGAAGGCTTTCAAGTGAAA, TRC0000007181; *PSMC2* shRNA-2, 5′ GCCAGGGAGATTGGATAGAAA, TRC0000007183; *PSMC2* shRNA-3, 5′ GCCTGCCTTATCTTCTTTGAT, TRC0000007184; *PSMC2* shRNA-4, 5′ CCTAAGATTGACCCAACAGTT, TRC0000007185, *LacZ* shRNA, 5′ TGTTCGCATTATCCGAACCAT, TRCN0000231726.

Cell Culture

Cancer cell lines were genotyped as part of the Cancer Cell Line Encyclopedia (Barretina et al., 2012). The generation of immortalized ovarian surface epithelial cells was previously described (Liu et al., 2004). TYKNU and HEYA8 were cultured in DMEM supplemented with 10% Fetal bovine serum and 2 mM L-Glutamine and all the remaining cell lines were cultured in RPMI 1640 supplemented with 10% Fetal bovine serum.

Lentivirus Production

Lentiviruses were produced for expression constructs or shRNA constructs in 293T cells cultured in DMEM with 10% FBS supplemented with 4 mM L-Glutamine using the three-vector system as described (Moffat et al., 2006). The virus was diluted (1:10) and added to 2×10^5 cells in a 6 well plate containing 8 μg/ml of polybrene (Sigma). Plates were centrifuged for 15 min, 1126 X *g* at room temperature. For selection of virally infected cells 24 hr postinfection 2 μg/ml of Puromycin (LKO.1) or 10 μg/ml of Blasticidin (LEX303) was added. Where applicable, lysate was collected and protein levels were analyzed 5 d after infection.

Inducible *PSMC2*-Specific shRNA System

Sense-antisense oligonucleotides (IDT) were annealed and then cloned into Tet-pLKO-neo (Addgene #21916) (AgeI/EcoRI) as follows: *PSMC2* shRNA-2, Sense 5′CCGGGCCAGGGAGATTGGATAGAAACTCGAGTTTCTATCCAATCTCCCTGGCTTTTTG, Antisense 5′AATTCAAAAAGCCAGGGAGATTGGATAGAAACTCGAGTTTCTATCCAATCTCCCTGGC; *PSMC2* shRNA-3, Sense 5′CCGGGCCTGCCTTATCTTCTTTGATCTCGAGATCAAAGAAGATAAGGCAGGCTTTTTG, Antisense 5′AATTCAAAAAGCCTGCCTTATCTTCTTTGATCTCGAGATCAAAGAAGATAAGGCAGGC; *LacZ* shRNA, Sense 5′CCGGTGTTCGCATTATCCGAACCATCTCGAGATGGTTCGGATAATGCGAACATTTTTG, Antisense 5′AATTCAAAAATGTTCGCATTATCCGAACCATCTCGAGATGGTTCGGATAATGCGAACA.

Plasmid sequences were confirmed by sequencing. Lentiviruses generated using these constructs were used to infect either OVCAR8 or A2780 cells. Stably infected cells were selected with Geneticin (500 ug/ml) (Sigma). Cells were treated with 100 ng/ml of doxycycline unless otherwise indicated (Sigma). Beginning 4 d after the addition of doxycycline, OVCAR8 cells begin to die. Therefore, to assess the level of PSMC2 suppression in OVCAR8 cells, we collected cells 3 d after the addition of doxycycline. Because the proliferation and viability of A2780 cells, in contrast, are not affected by the addition of doxycycline, we collected cells 4 d after the addition of doxycycline at which point PSMC2 levels had achieved a new steady state. All proliferation or viability studies on both cell lines were conducted 7 d after the addition of doxycycline. Lysates from cells using this system were made in Buffer A for all immunoblots except for Ubiquitin immunoblots, which were made in Buffer B.

Ectopic V5-PSMC2 Expression

PSMC2 was engineered with a V5 sequence at the N terminus and cloned into pLEX303. To minimize a second translation initiation site that used the endogenous ATG, we amplified PSMC2 using a 5′ primer that contained a sequence that would code for the V5 epitope and also mutated the endogenous methionine to a threonine. The sequence of the exogenous construct added the following amino acids to the N-terminus (MGKPIPNPLLGLDST) where the final T (Threonine) is in place of the endogenous methionine. No modifications were made to the C terminus. OVCAR8 or IOSE cells were serially infected with lentiviruses containing either pLEX303 GFP (obtained from the TRC) or pLEX303 V5-PSMC2. Repeat infections were performed with respective constructs until the expression of ectopic V5-PSMC2 (as measured by immunoblot) was comparable to the endogenous protein. OVCAR8 cells that expressed either V5-PSMC2 or GFP were infected with lentivirus that express *PSMC2* shRNA-1 or shLacZ in pLKO.1. 5 d after infection, the cells were analyzed by immunoblot and 7 d after infection, in triplicate the cells were analyzed for total ATP content (Promega). Relative ATP content was normalized to the cells infected with shLacZ. Cell lines used for orthotopic xenograft tumors were engineered to express firefly luciferase. Lentiviruses made from vectors containing the luciferase gene (pLEX301) and obtained from the TRC were used to infect the indicated cell lines.

Protein Lysates

All cells were harvested and pelleted in cold PBS. All subsequent procedures were performed at 4°C. For lysate generated in "Buffer A," the cell pellet was resuspended in 10% Glycerol, 25 mM HEPES pH 7.4, 10 mM $MgCl_2$, 1 mM ATP, 1 mM DTT, and phosphatase and protease inhibitors without EDTA (Roche). Sonication was performed at low intensity using a micro-tip on ice for 1 min (50% cycle). The resulting cell mixture was centrifuged at 13000 X *g* for 15 min at 4°C. The supernatant was collected and centrifuged at 100,000 X *g* for 60 min. The subsequent supernatant was collected and used in future studies as lysate. Protein amount was normalized using the Bradford reagent (Bio-Rad). For lysate generated in "Buffer B," the cell pellet was resuspended in 20 mM Tris-HCL pH 7.5, 150 mM NaCl, 10% Glycerol, 1% Triton-X, 0.2 mM DTT, 250 μg/ml NEM supplemented with protease inhibitors

(Roche) and Phosphatase Inhibitors (PhosStop -Roche). Samples were incubated for 15 min and supernatants were collected after centrifugation at 15,000 X *g*. Finally, for lysate generated in "RIPA," the cell pellet was resuspended in 1X RIPA buffer (Boston Bioproducts) that was supplemented with protease inhibitors with EDTA (Roche) for 15 min. The supernatant was collected after centrifugation at 15,000 X *g* for 15 min. Protein lysates made in RIPA or Buffer B were normalized with THERMO BCA normalization kit (Bio-Rad), using a BSA standard curve. Lysate analysis of 26S proteasome components across ovarian cancer cell lines and PSMC2 levels following shRNA expression were generated in RIPA buffer. For all experiments that involved native analysis of the proteasome, lysate was made in Buffer A and then analyzed either in non-denaturing or denaturating (SDS loading buffer) conditions.

Purification of Complex^{PSMC2} and the 26S Proteasome

Continuous glycerol gradients (from 10%–40%) were made in 25 mM HEPES pH 7.4, 10 mM $MgCl_2$, 1 mM ATP, 1 mM DTT. 18 mg of lysate (Buffer A) was loaded at the top of a 14 ml gradient and centrifuged for 20 hr at 195,000 x *g*. Fractions were removed from top of each gradient in 1 ml increments. Native PAGE described above was used to determine which fractions contained Band A or 26S proteasome and the indicated pooled fractions were then pooled and incubated with Anti-V5 agarose conjugates. Immunoprecipitates were eluted with 20 μg/ml of V5 peptide overnight at 4°C and analyzed by immunoblot.

Immunoprecipitation of Complex^{PSMC2} and the 26S Proteasome

Immunoprecipitation was performed by incubating fractions with 50 μl of Anti-V5 agarose conjugated beads (Sigma) and rotating for 16 hr at 4°C. Each wash step began with centrifugation at 1,000 X *g* for 3 min, removal of the supernatant, and resuspension of the beads in 1 ml of buffer A. Three washes were completed and the samples were then incubated in 100 μl of 20 μM V5 peptide (Sigma) in buffer A. Equal volumes were then denatured in SDS loading buffer and analyzed by immunoblot.

Determination of *PSMC2* mRNA Levels

Cells were harvested and pelleted in PBS. RNA was extracted from cell pellets and resuspended in Trizol Reagent (Invitrogen) according to manufacturer's protocol. The precipitated total RNA was then resuspended in 0.1 ml of a 1x TurboDNase buffer with 2U of DNase (Ambion) and incubated at 37°C for 15 min. RNA was then purified using the QIAGEN RNEasy kit according to manufacturer's instructions for "RNA Clean Up." 1 μg of RNA was used to generate cDNA using the M-MLV Reverse Transcriptase kit (Invitrogen) according to the recommended protocol. PCR reactions were performed in replicates of five using SybR PCR master mix (Applied Biosystems) and Ct values were automatically determined using Applied Biosystems 7300 System software. The resulting data were normalized to housekeeping genes and analyzed using the delta-delta Ct method for fold difference between control and test samples. Unless otherwise indicated *PGK1* was used as an internal control. Primers used in quantitative RT-PCR are as follows: *PGK1* (5′AGAGGGAGCCAAGATTGTCA, 5′ GGTATGCCAGAAGCCACAGT), *Tubulin* (5′TCTGTTCGCTCAGGTCCTTT, 5′ TGTGTCCTTGCACCCAAATA), and *PSMC2* (5′ TCCACCCGGTACAGGCAAGACACT, 5′ CGAGCCCCCTCACCGACGTA).

PSMC2 siRNA Experiments in A2780 Cells

5×10^5 cells were plated in 10 cm plates on Day 0. Each plate was transfected with a total of 500 pmol of siRNA and 20 μl lipofectomine RNAi Max (Invitrogen) using the manufacturer's recommended procedure. Three pre-annealed PSMC2 siRNAs were obtained from IDT DNA and pooled in equimolar ratios: siRNA-1 (5′-GCUGUAAAUAAGGUCAUUAAGUCTT, 5′-AAGACUUAAUGACCUUAUUUACAGCUU), siRNA-2 (5′-AGAUAAUCAAUGCUGAUUCGGAGGA, 5′-UCCUCCGAAUCAGCAUUGAUUAUCUUU), siRNA-3 (5′-CCCACAUAUUUAAGAUUCACGCUCG, 5′-CGAGCGUGAAUCUUAAAUAUGUGGGUC). The concentration of the pool was varied and the difference was made up with control siRNA (Ambion). 24 hr after transfection, 2.5×10^5 viable cells (determined by trypan blue) were plated in duplicate for a six-day proliferation assay. The remaining cells were plated and harvested for lysate (RIPA) 3 d after transfection.

PSMC2 siRNA Experiments in A2780-Dox Cells

1.5×10^6 of A2780-Dox-shLacZ and A2780-Dox-shRNA-2 cells were plated in 10 cm plates on Day 0, two for each cell line. On Day 1, the media from one plate of each cell line was replaced with media containing 100 ng/ml of doxycycline. On day 2, these cells were passaged into 96 well plates at 2,500 cells/well, as well as a single 10 cm plate (to be used for RNA) for each condition and cell line. On Day 3, these cells were transfected with 0.2 mM lipofectomine RNAi Max (Invitrogen) along with siRNA at a total concentration of 20 nM, with varying levels of siRNA specific for either *PSMC2* or *PSMC5* using the manufacturer's recommended procedure. *PSMC2* siRNA are listed above, with additional *PSMC5* siRNAs obtained from IDT DNA predesigned siRNA (Catalog # HSC.RNAI.N002803.12.1, HSC.RNAI.N002803.12.2, HSC.RNAI.N002803.12.3) and pooled in equimolar ratios. The concentration of the pool was varied and the difference was made up with control siRNA (Ambion). Proliferation was measured by cell titer glo, and qRT-PCR data were used to determine concentrations where siPSMC2 (2.5 nM) and siPSMC5 (5 nM) led to similar levels of suppression of their respective targets.

Bortezomib Sensitivity Experiments

Throughout the experiment, A2780 cells engineered in the *PSMC2* shRNA inducible system were either treated with vehicle or 30 ng/ml of doxycycline. Doxycycline treatment was started on Day 0. On day 4, cells were plated at 2,000 cells/ well in a 96 well plate. The following day, the cells were treated with varying concentrations of bortezomib or vehicle. Total ATP levels were measured

by Cell Titer Glo (Promega) 72 hr after adding bortezomib. The data were normalized to the vehicle treated sample. Graphpad was used to determine the IC_{50} by constructing a non-linear regression with a four-parameter variable slope.

Cell Cycle and Apoptosis Assays Using the *PSMC2* shRNA Inducible System

We cultured either A2780 or OVCAR8 cells engineered with our *PSMC2* shRNA inducible system in the presence or absence of doxycycline (100 ng/ml) and collected them for analysis after 3 d. We used the BrdU Flow Kit (BD Pharmigen) according to manufacturer's protocol to determine the percentage of cells in each phase of the cell cycle 72 hr after the addition of doxycycline. At the same time point, we independently determined the number of cells undergoing apoptosis by FACS analysis of Annexin-5 according to the manufacturers recommended procedure (Invitrogen V13241).

PSMC2 and Control siRNA TPN Sequences

Sequences of siRNA used for TPN are as follows: *PSMC2* siRNA-1, Sense 5′- GCUGUAAAUAAGGUCAUUAUU, Antisense 5′- UAAU GACCUUAUUUACAGCUU, *PSMC2* siRNA-2, Sense 5′- GCCAGGUGUACAAAGAUAAUU, Antisense 5′- UUAUCUUUGUACACCUG GCUU, *PSMC2* siRNA-3, Sense 5′- GGACCCACAUAUUUAAGAUUU, Antisense 5′- AUCUUAAAUAUGUGGGUCCUU, *GFP* siRNA, 5′-GGCUACGUCCAGGAGCGCA, 5′-UGCGCUCCUGGACGUAGCC.

SUPPLEMENTAL REFERENCES

Moffat, J., Grueneberg, D.A., Yang, X., Kim, S.Y., Kloepfer, A.M., Hinkle, G., Piqani, B., Eisenhaure, T.M., Luo, B., Grenier, J.K., et al. (2006). A lentiviral RNAi library for human and mouse genes applied to an arrayed viral high-content screen. Cell *124*, 1283–1298.

Ortiz-Estevez, M., De Las Rivas, J., Fontanillo, C., and Rubio, A. (2011). Segmentation of genomic and transcriptomic microarrays data reveals major correlation between DNA copy number aberrations and gene-loci expression. Genomics *97*, 86–93.

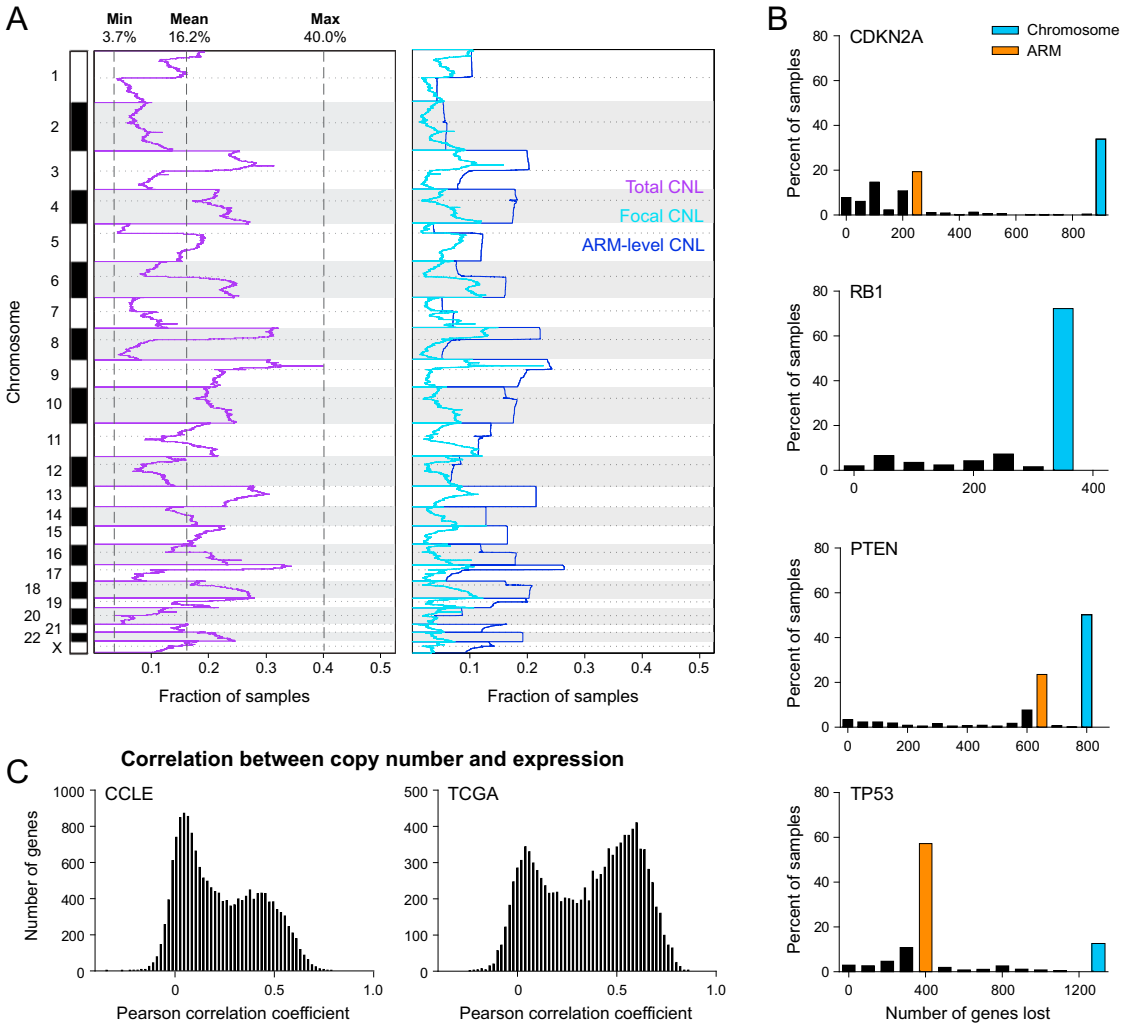

Figure S1. Characterization of Copy Number Loss in Human Cancer, Related to Figure 1

(A) Frequency of copy number loss across the genome among 3,131 cancers. The total frequency (purple, left panel) and frequencies due to focal (blue) and arm-level (teal) events (right panel) are shown. Thresholds and methods for calling losses were as previously described (Mermel et al., 2011).

(B) Number of genes affected by copy loss events that include prominent tumor suppressor genes. For each sample where the indicated tumor suppressor gene underwent copy number loss, we calculated the number of genes affected by the largest copy loss event affecting that gene. The results are plotted as a histogram.

(C) Strength of correlation between copy number and mRNA expression level across genes profiled in the CCLE and TCGA ovarian cancer data sets. Results represent Pearson correlation coefficients between $\log_2$ copy number levels and quantile normalized mRNA levels for 16,767 genes across 806 cell lines in the CCLE (Barretina et al., 2012) and 11,119 genes across 429 ovarian tumors from the TCGA (Cancer Genome Atlas Research Network, 2011). In consonance with prior reports from other data sets (Ortiz-Estevez et al., 2011), the correlation between copy number and expression revealed that genes fall into one of two classes: a class in which mRNA levels are relatively independent of copy number (CCLE: modal r = 0.05; TCGA: modal r = 0.07), and a second class in which copy number and gene expression are more closely correlated (CCLE: modal r = 0.49; TCGA: modal r = 0.61). We found that CYCLOPS candidates were enriched in the latter class (CCLE p = 0.0004; TCGA p = 0.04). Notably, among all 158 KEGG pathways, the three pathways most enriched in CYCLOPS candidates also have significant correlations between copy number and expression: spliceosome (CCLE r = 0.46, FDR = $2.2\text{x}10^{-5}$; TCGA r = 0.56, FDR = 3.9×10^{-5}), proteasome (CCLE r = 0.52, FDR = $2.2\text{x}10^{-5}$; TCGA r = 0.60, FDR = 3.9×10^{-5}) and ribosome (CCLE r = 0.44, FDR = $2.2\text{x}10^{-5}$; TCGA r = 0.47, FDR = $1.1\text{x}10^{-4}$). These observations indicate that mRNA expression of CYCLOPS genes is reduced as a result of copy loss, a feature also shared by other members of CYCLOPS-enriched pathways.

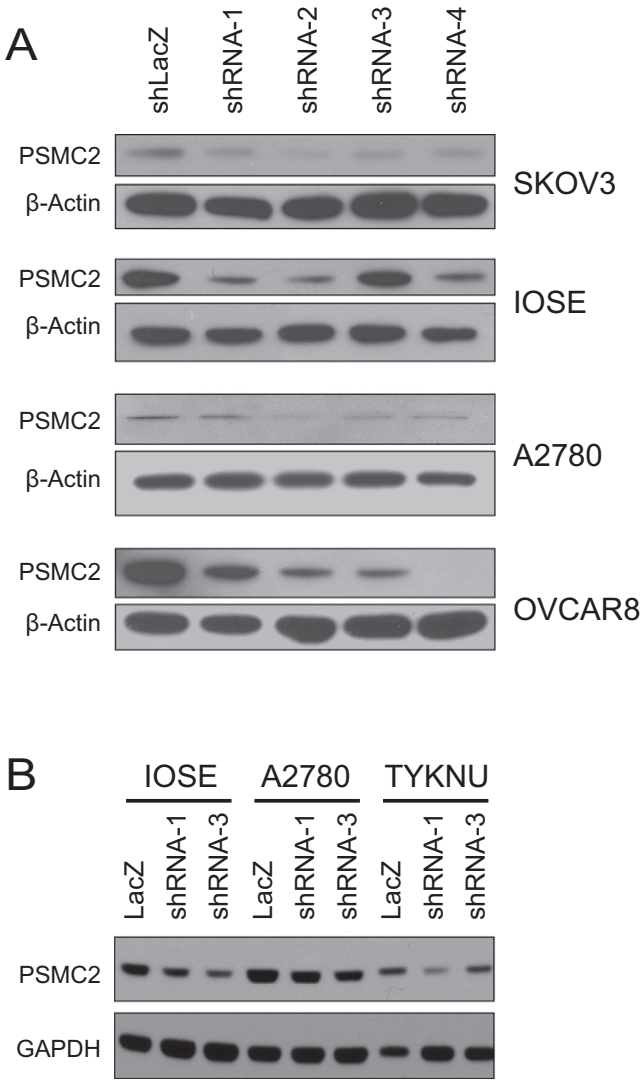

Figure S2. PSMC2 Suppression by RNAi, Related to Figure 2

(A) *PSMC2* suppression in ovarian cell lines. We individually expressed all four *PSMC2* shRNAs and a control shRNA, shLacZ. Among the four *PSMC2* shRNAs, *PSMC2* shRNA-2, 3, and 4 were used by ATARiS to calculate the *PSMC2* dependency score and exhibited consistent suppression of PSMC2. Note that comparisons between the extent of PSMC2 suppression across cell lines cannot be made from these data due to differences in exposure; more accurate comparisons are made in Figure S3F.

(B) PSMC2 levels in cells that express shLacZ or *PSMC2* specific shRNA from a single lentiviral integrant.

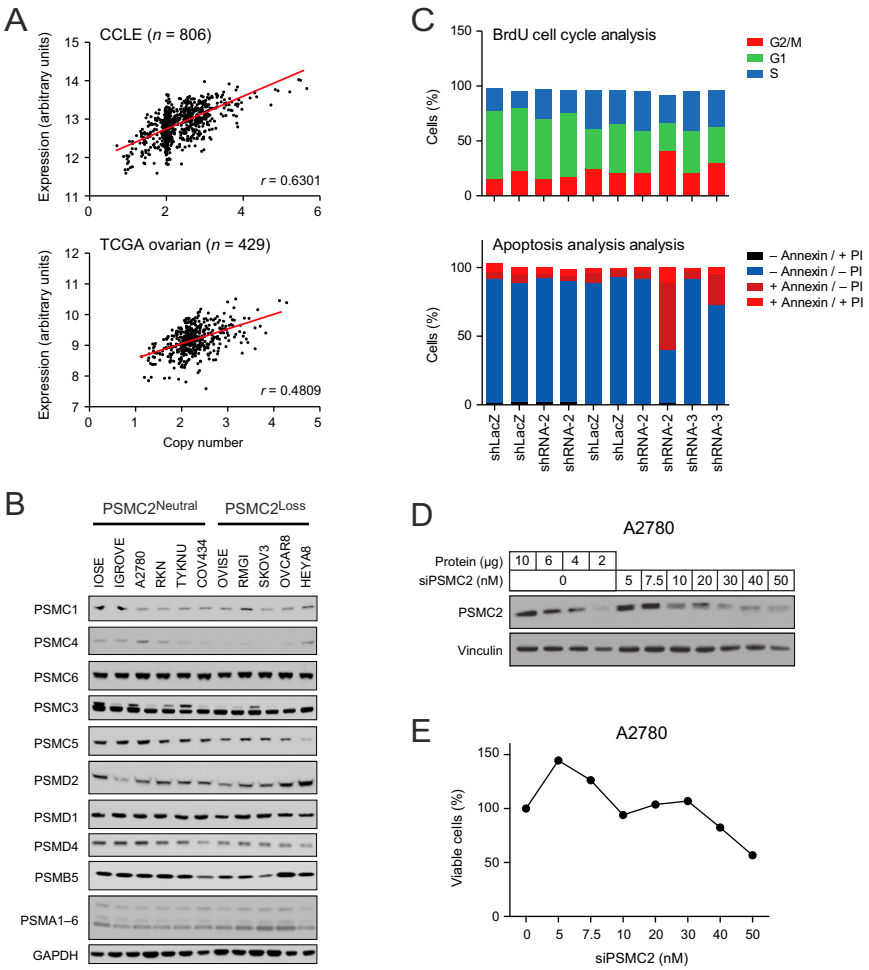

Figure S3. PSMC2 Expression Levels and Sensitivity to Suppression, Related to Figure 3

(A) Scatterplots of PSMC2 copy number versus mRNA expression derived from cell lines in CCLE (Barretina et al., 2012) and primary ovarian tumors in TCGA (Cancer Genome Atlas Research Network, 2011). A linear regression line and the Pearson correlation coefficient (r) are also displayed.

(B) Comparison between *PSMC2* copy number and protein expression of ten other 26S proteasome components.

(C) Flow cytometry measurements of cell cycle progression (top) and apoptosis (bottom) in $PSMC2^{Neutral}$ and $PSMC2^{Loss}$ cells with and without suppression of *PSMC2*. No differences in cell cycle progression were observed, but $PSMC2^{Loss}$ cells undergo increased Annexin V staining, indicating increased apoptosis, after *PSMC2* suppression.

(D) PSMC2 expression in A2780 cells after transfection with varying concentrations of siPSMC2. The four left-most lanes of the immunoblot represent a dilution series of cells transfected with a control siRNA for comparison.

(E) Viability of cells in (D) determined by Trypan blue exclusion.

(F) Relative Difference in PSMC2 levels between cell lines. The immunoblot indicates PSMC2 levels in OVCAR8 cell lysates relative to a dilution series using A2780 cell lysates.

(G) Relative *PSMC2* mRNA expression between OVCAR8 and A2780 cells. The comparison between mRNA levels was performed by quantitative RT-PCR and we used the average value of two different internal controls, *Tubulin* and *PGK1*.

(H) Relative levels of *PSMC2* (top) or *PSMC5* (bottom) mRNA in cells transfected with siRNA that target the indicated gene. Data are presented as average ±SD

(I) Relative mRNA level of proteasome components in conditions where PSMC2 is suppressed (with doxycycline) to those where it is not (no doxycycline). Data are presented as an average ratio ±SE.

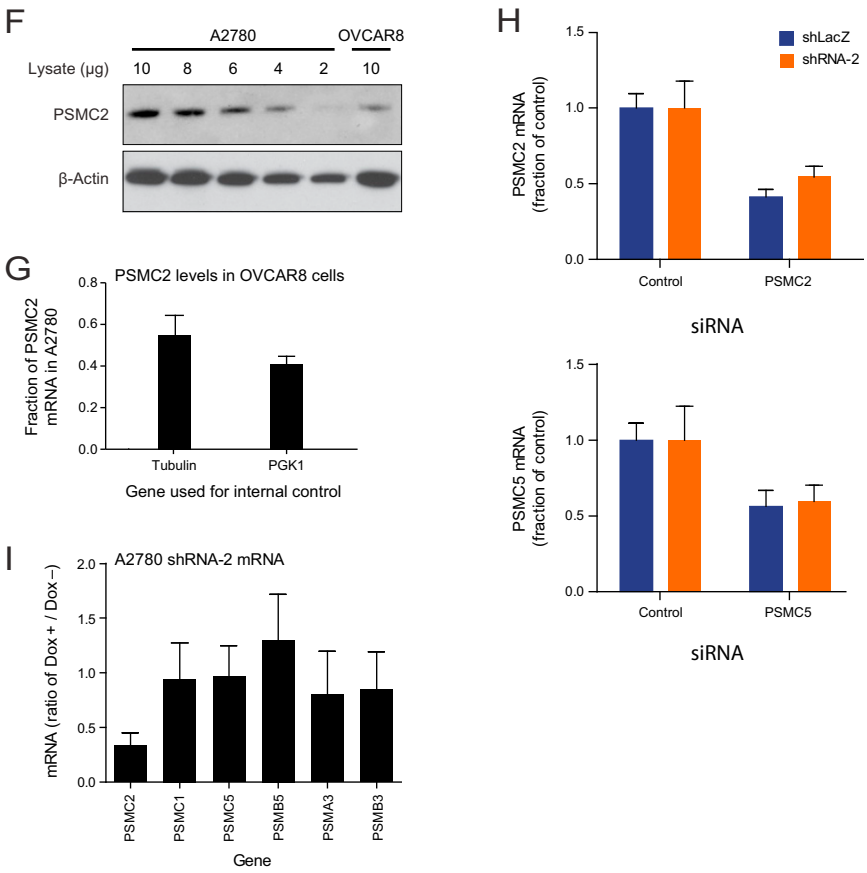

Figure S3. ***(continued)*.**

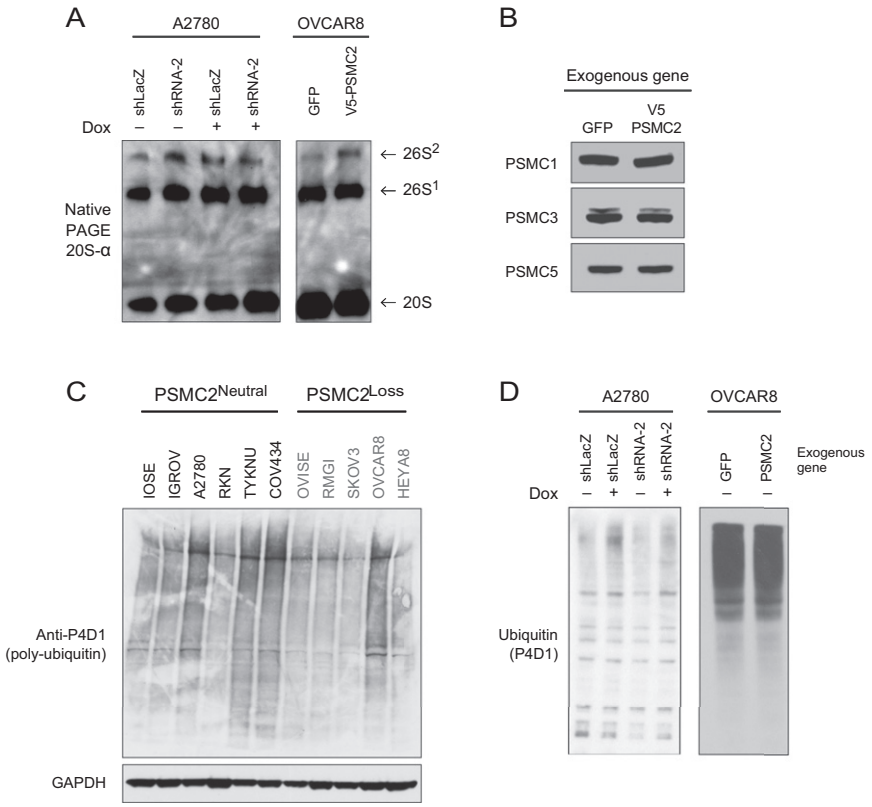

Figure S4. *PSMC2* Copy Number Loss and 26S Proteasome Function, Related to Figure 4

(A) Longer exposure of native gel immunoblot for PSMA1–6 showing minor changes in $26S^2$ proteasome content in response to changes in PSMC2 levels.

(B) Expression of exogenous V5-PSMC2 in $PSMC2^{Loss}$ cell line does not increase the levels of other 19S proteins.

(C) Polyubiquitinated protein levels in $PSMC2^{Neutral}$ and $PSMC2^{Loss}$ cells.

(D) Decreased levels of PMSC2 in $PSMC2^{Neutral}$ cells or increased expression of PSMC2 in $PSMC2^{Loss}$ cells does not qualitatively affect polyubiquitinated protein levels.

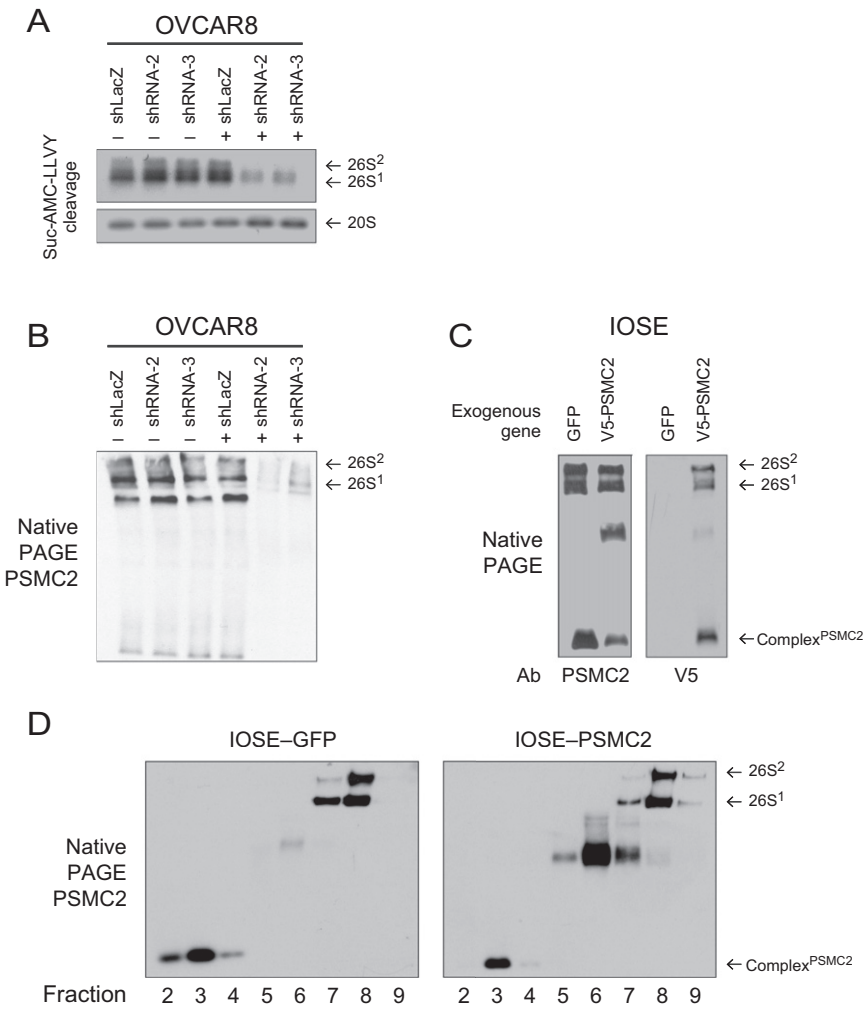

Figure S5. PSMC2 Suppression and 26S Proteasome Function, Related to Figure 5

(A and B) OVCAR8 cells with and without *PSMC2* suppression analyzed by Native PAGE immunoblots for (A) in gel 26S complex peptidase cleavage and (B) PSMC2.

(C) Native PAGE immunoblots with anti-PSMC2 (left) and anti-V5 (right) of IOSE cells that express either GFP or V5-PSMC2.

(D) Glycerol gradient (10%–40%) fractionation of IOSE-V5-GFP (left) and IOSE-V5-PSMC2 (right) lysate. Fractions were analyzed using Native PAGE and immunoblotted for PSMC2.

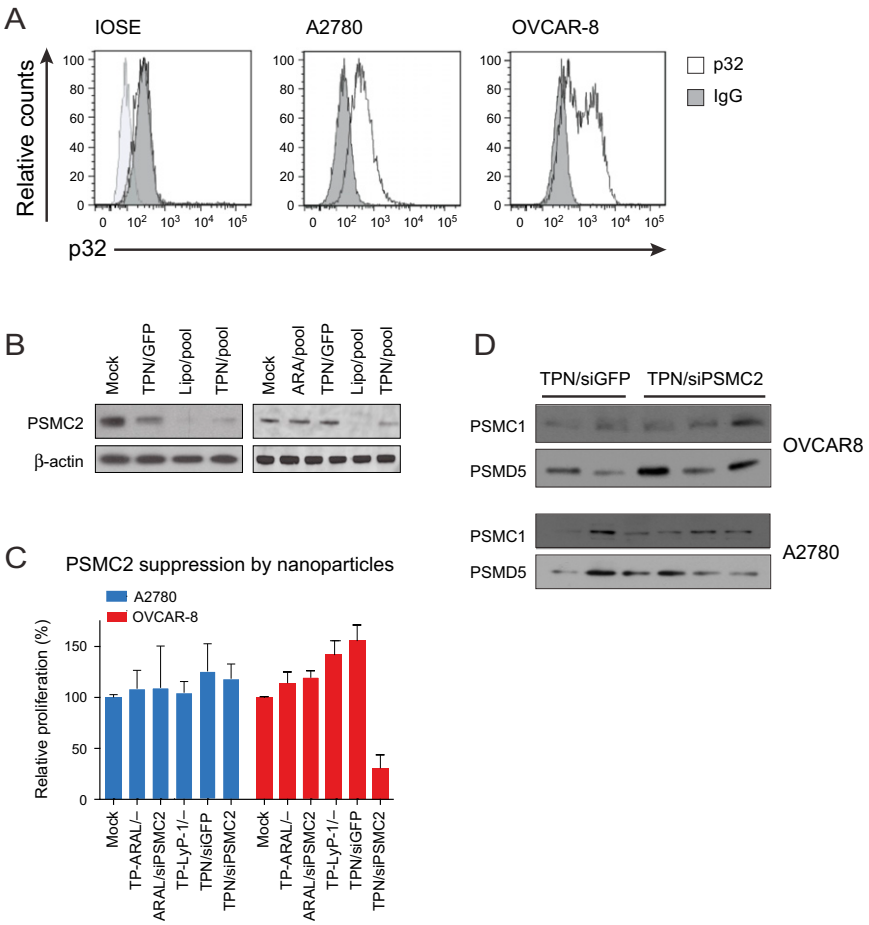

Figure S6. Tumor-Penetrating Nanoparticle Leads to PSMC2 Suppression, Related to Figure 6

(A) FACS analysis of p32 surface expression on A2780 and OVCAR8 cells.

(B) Immunoblots of PSMC2 in A2780 and OVCAR8 cells with and without in vitro TPN-mediated delivery of *PSMC2*-siRNA.

(C) Proliferation of A2780 and OVCAR8 cells after treatment in vitro with siGFP or siPSMC2 using either the TPN or a nanoparticle containing the scrambled peptide (ARA), relative to mock controls.

(D) The levels of other components of Complex^{PSMC2}, PSMC1 and PSMD5, in orthotopic tumors treated with different nanoparticles.